Fall 1-31-2015

Petri net models of microgrids with distributed generators

Xiaoyu Lu
New Jersey Institute of Technology

ABSTRACT

**PETRI NET MODELS OF MICROGRIDS
WITH DISTRIBUTED GENERATORS**

**by
Xiaoyu Lu**

This thesis introduces some basic concepts and control methods about a microgrid. Then, two hot issues are investigated. One is how to control multiple distributed generators; and another is how to model both discrete event and continuous behaviors of a microgrid. To address these two issues, this thesis work applies Petri nets to both modeling and control of a microgrid. Ordinary Petri nets, hybrid Petri nets, and finite capacity Petri nets, are introduced with their examples targeted at modeling the behavior of a microgrid. Coordination control of multiple distributed generators based on a Petri net model is proposed. Compared with multi-V/f control, the Petri net based control enables the system to operate with a longer stable time interval. Finally, a hybrid Petri net model is constructed to model both discrete event and continuous behaviors of an on-load tap changing transformer system. Compared with an algebraic method, the hybrid Petri net offers a clear and easy-to-understand method to describe such a system.

PETRI NET MODELS OF MICROGRIDS
WITH DISTRIBUTED GENERATORS

by
Xiaoyu Lu

A Thesis
Submitted to the Faculty of
New Jersey Institute of Technology
in Partial Fulfillment of the Requirements for the Degree of
Master of Science in Electrical Engineering

Department of Electrical and Computer Engineering

January 2015

Blank Page

**PETRI NET MODELS OF MICROGRIDS
WITH DISTRIBUTED GENERATORS**

Xiaoyu Lu

Dr. Mengchu Zhou, Thesis Advisor	Date
Distinguished Professor of Electrical and Computer Engineering, NJIT	

Dr. Walid Hubbi, Committee Member	Date
Associate Professor of Electrical and Computer Engineering, NJIT	

Dr. Qi Kang, Committee Member	Date
Associate Professor of School of Electronics and Information, Tongji University	

BIOGRAPHICAL SKETCH

Author: Xiaoyu Lu

Degree: Master of Science

Date: January, 2015

Undergraduate and Graduate Education:

- Master of Science in Electrical Engineering,
  New Jersey Institute of Technology, Newark, NJ, 2015

- Bachelor of Science in Electrical Engineering and Automation,
  Nanjing University of Technology, Nanjing, P. R. China, 2011

Major: Electrical Engineering

Dedicated to my family, all inclusive, known and unknown –for giving birth to me at the first place and supporting me spiritually throughout my life.

ACKNOWLEDGMENT

Foremost, I would like to express my deepest gratitude to my advisor, Dr. Mengchu Zhou, for excellent guidance and patience. Professor Zhou served as my research advisor, but he was very influential in the academic path choice I have made and gave me many excellent suggestions.

I would also like to thank Dr. Walid Hubbi for giving me his deep knowledge of power systems and Dr. Qi Kang for his advice to my research.

My sincere thanks also go to my group members, Yan Qiao and Jingchu Ji, and my good friends, Wenhan Lu, Chongming Liu, Xilong Liu and Yi Wang, for giving me many excellent suggestions and assisting me in completing this thesis work.

TABLE OF CONTENTS

LIST OF TABLES

LIST OF FIGURES

LIST OF SYMBOLS

●   Token

○   Discrete Place

◎   Continuous Place

▬   Discrete Transition

▭   Continuous Transition

CHAPTER 1

INTRODUCTION

Due to the constraint of fossil fuel and rising environment pollution, the world witnesses the increasing demand for affordable sustainable energy systems. Their wide use can improve the structures of energy supply from clean and renewable sources. Energy sources can be divided into two categories as non-renewable energy and renewable energy. Since the depletion of non-renewable energy resources, such as oil, coal sources and natural gas, is inevitable, people now turn to Renewable Energy Resources (RES) that can resupply themselves, such as solar, wind, hydropower, biomass and geothermal energy. During the last few decades, the development of renewable energy sources received a significant amount of attention around the world.

1.1 Renewable Energy Sources

Renewable energy is a source that can be used to reduce the negative effects of using fossil fuels. With the economic growth, urbanization and energy needs of industries, global energy demand is expected to be doubled by 2050 [Aydin, 2014]. Underscoring the need for higher energy supply to meet demand worldwide, RES seem to be one of the best solutions to deal with energy shortage.

Table 1.1 2000-2012 Clean Energy Market

Year	Solar PV (InBillions)	Wind Power (InBillions)	Biofuels (InBillions)
2000	2.5	4.0	N/A
2001	3.0	4.6	N/A
2002	3.5	5.5	N/A
2003	4.7	7.5	N/A
2004	7.2	8.0	N/A
2005	11.2	11.8	15.7
2006	15.6	17.9	20.5
2007	20.3	30.1	25.4
2008	29.6	51.4	34.8
2009	36.1	63.5	44.9
2010	76.2	60.5	56.4
2011	91.6	71.5	83
2012	79.7	73.8	95.2

Source: Aydin, B. (2014). SWOT analysis of renewable energy. In *Proc of 2014 IEEE International Conference and Utility Exhibition on Green Energy for Sustainable Development (ICUE)* (pp. 1-7).

In Table 1.1, the market values of three RES (solar energy, wind and biofuels) from 2000 to 2012 are listed. In 2000, the market value of renewable energy was USD 6.5 billion. It reached USD 75.8 billion in 2007. Final market value reached USD 248.7 billion in 2012 and it is estimated to reach USD 426.1 billion in the year of 2022. From its increasing market value, the renewable energy is expected to experience very rapid growth.

According to the data from year 2012, renewable power represents 21.7% of world electric production. Table 1.2 shows total investment made to renewable energy in years 2010 - 2012. The total renewable energy capacity is increasing gradually as shown in Table 1.2. Wind power and solar power are two hot RES areas.

Table 1.2 2010-2012 Renewable Energy

Year		2010	2011	2012
Investment in new renewable capacity (annual)	billion USD	227	279	244
Renewable power capacity (total, not including hydro)	GW	315	395	480
Renewable power capacity (total, including hydro)	GW	1250	1355	1470
Hydropower capacity (total)	GW	935	960	990
Solar PV capacity (total)	GW	40	71	100
Wind power capacity (total)	GW	198	238	283

Source: Aydin, B. (2014). SWOT analysis of renewable energy. In *Proc of 2014 IEEE International Conference and Utility Exhibition on Green Energy for Sustainable Development (ICUE)* (pp. 1-7).

1.1.1 Wind Power

Wind power sources have given the least negative effect to the environment. Top four countries utilizing wind power around the world are: U.S with 13124 MW capacity, China with 12960 MW capacity, Germany with 2415 MW capacity, and India with 2336 MW capacity. While the wind power capacity was 1280 MW by the end of the year 1996, annual installation reached the capacity 44799 MW in 2012 as shown in Figure 1.1. Total installed capacity of wind power since 1996 was 283 GW in 2012.
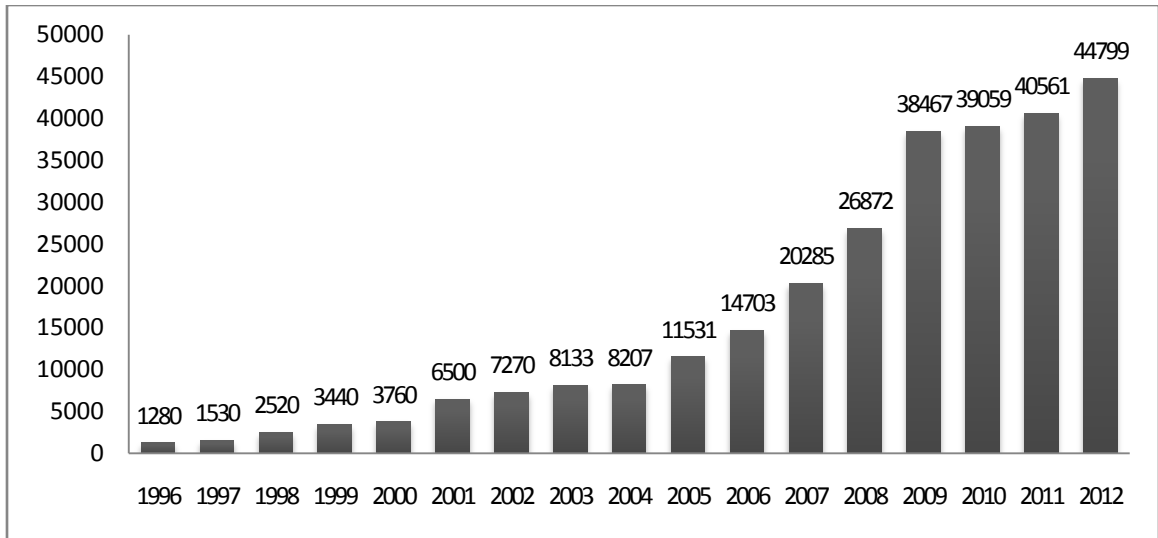
Figure 1.1 1996-2012 Wind power capacity.

Source: Aydin, B. (2014). SWOT analysis of renewable energy. In *Proc of 2014 IEEE International Conference and Utility Exhibition on Green Energy for Sustainable Development (ICUE)* (pp. 1-7).

A wind turbine is the device that converts kinetic energy from the wind into electrical power. Normally, the wind turbine is installed at the location with high wind speed, such as coastline. Arrays of wind turbines are known as a wind farm that is becoming an important part of power supply.

1.1.2 Solar Power

Solar power results from the conversion of sunlight and heat with no pollution. As seen in Table 1.2, solar capacity was 40 GW in 2010. By the end of 2011, a total of 67.4 GW had been installed. At year 2012, the capacity reached 100 GW. Following hydro and wind power, solar photovoltaic energy sources are now the third most important renewable energy.

A photovoltaic (PV) cell is the device that converts sunlight into electricity by the photoelectric effect. Currently, with the development of technology, the conversion efficiency exceeds 20% while the efficiency value was 4.5-6% in 1960s. In the lab, this

efficiency can reach 40%. Unlike the location constraints for wind turbines and hydro generators, PV panels can be installed in any places where sunlight is sufficient, such as the roof of houses and top of the streetlight [Molina, 2008] [Wang, 2013]. Comparing with wind turbines, PV panels can operate with less maintenance and less reduction of conversion efficiency.

1.2 Microgrid

1.2.1 Basic Concept of Microgrids

Microgrids are proposed for effective integration of distributed generators (DGs), energy storage systems and loads to the utility grid to provide high quality and high reliability electric power for the end-users [Chan, 2011]. Almost all microgrids are located near the loads. Also, a microgrid is proper to be built for remote rural communities adopting the advantage of its self power supply. By locating a distributed generator near the load, transmission and distribution costs are decreased and delivery problems are mitigated. Normally, a microgrid is connected to the main grid via the point of common coupling (PCC). It has two operating modes. One is a grid connected mode, while the other is an islanded mode. The ideal microgrid can supply reliable power whether the microgrid is operated at a grid connected or islanded mode [Peas, 2005].

A grid connected mode is the normal operating mode of a microgrid. In this mode, the microgrid is connected to the main grid. The whole microgrid must be operated synchronously with the main one. The latter can compensate the microgrid when the DGs inside the microgrid are of shortage to meet the local load demand. On the opposite,

because DGs make full use of renewable energy, a microgrid can send energy to main grid that may decrease the consumption of fossil fuel.

In an islanded mode, a microgrid is disconnected from the upstream distribution network due to fault or high disturbance occurrence in the main grid. The microgrid operates autonomously, in a similar way to a physical island. It is because a microgrid can run in an autonomous operating mode. The research on microgrids has been paid much attention as a means to improve the performance of electrical power since the 2003 northeast blackout.

1.2.2 Importance of Microgrids

According to [Hartono, 2013] and [Banerji, 2013], the importance of a microgrid can be described in the following aspects:

1. It has reliable power supply to the microgrid region during natural disasters, blackout etc.
2. A microgrid has less power loss due to a transmission system if the microgrid is able to respond to the local load demand.
3. Its reliability and high quality of power can be enjoyed by a customer.
4. A microgrid yields environmental benefits with renewable energy being utilized as DGs.

Although the importance is mentioned above, a microgrid faces some issues to be addressed. First, in its islanded mode, how to control multiple DGs and stabilize the system without the support from a main grid is one of the hot issues. Second, how to model its discrete event dynamic behavior is another one. In this thesis, Chapter 2 discusses basic control methods for microgrids with multiple DGs. The concepts of ordinary Petri nets (PN), finite capacity Petri nets (FCPN) and hybrid Petri nets (HPN) are introduced in Chapter 3. Chapter 4 presents a mulit-V/f control method based on a Petri net model.

Chapter 5 proposes an HPN model for an On Load Tap Changing (OLTC) system to address the second issue. Chapter 6 concludes this thesis with a discussion of its limitations and future research directions.

CHAPTER 2

CONTROL OF MICROGRIDS

In a microgrid, there are many distributed generators (DGs). They are connected to the microgrid via inverters or transformers. Each of them needs a local controller. For the whole microgrid, a MicroGrid Central Controller (MGCC) is used to coordinate different controllers [Peas, 2005]. Currently, three basic control methods are popularly used. They are droop control, V/f control, where V represents voltage and f represents frequency, and P/Q control, where P represents active power and Q represents reactive power. Three commonly used coordination control methods are master-slave control, point to point control and hierarchical control.

2.1   Basic Control Methods

2.1.1 Droop Control

Droop control has widely been investigated by many research groups. A basic model of a microgrid, which contains one DG and one bus system only, is simplified into Figure 2.1. From its left side, there are a voltage source, inverter, filter and network system. The voltage source parallels with a capacitor to generate stable DC voltage output. The inverter is the one that converts DC to AC. The filter removes the disturbance from the inverter to the electrical network. The right side of Figure 2.1 is the electrical network. The resistance, inductance and capacitance of a cable are approximated into their equivalent impedance.
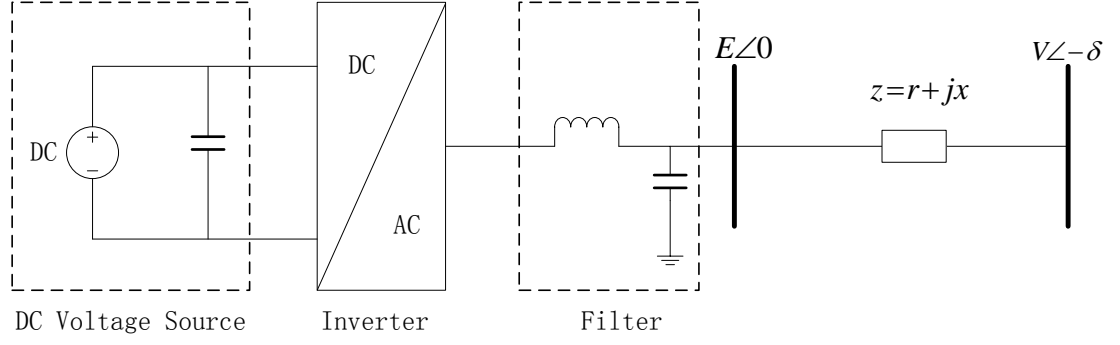
Figure 2.1 One DG and one bus system.

$E\angle 0$ is the terminal voltage of a DG. $V\angle -\delta$ is the voltage of a load bus. The impedance of a transmission line is described as $z = r + jx$. Figure 2.2 is the basic electrical circuit of a transmission system.
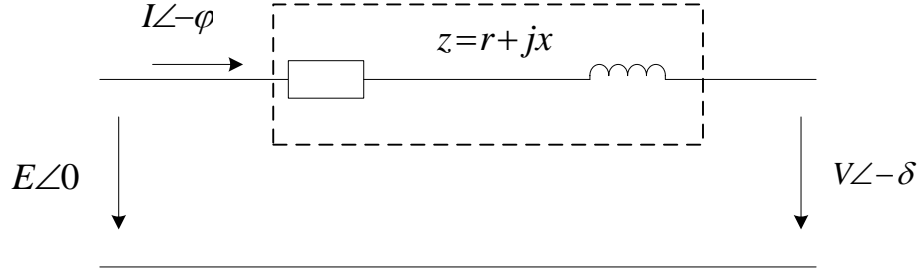
Figure 2.2 Basic electrical circuit of a transmission system.

We can obtain the equations about active power and reactive power as follows:

$$P = \frac{E}{r^2 + x^2} \times [r(E - V\cos\delta) + xV\sin\delta] \tag{2.1}$$

$$Q = \frac{E}{r^2 + x^2} \times [-rV\sin\delta + x(E - V\cos\delta)] \tag{2.2}$$

If $x \gg r$, these two equations can be simplified as follows:

$$P = \frac{E \times V}{x} \times \sin \delta \qquad (2.3)$$

$$Q = \frac{E^2 - EV \cos \delta}{x} \qquad (2.4)$$

If the power angel is small enough due to the transmission line of a microgrid that is short with less loss, the equations can be further simplified ($\sin \delta = \delta$ and $\cos \delta = 1$) as follows:

$$P = \frac{E \times V}{x} \delta \qquad (2.5)$$

$$Q = \frac{E^2 - EV}{x} = \frac{E(E - V)}{x} = \frac{E \cdot \Delta V}{x} \qquad (2.6)$$

From Equations (2.5) and (2.6), the relation between P and δ and that between Q and ΔV are obtained. At the same time, the relation between power angle and angle rate is shown as below:

$$\Delta \omega = \frac{d\delta}{dt} \qquad (2.7)$$

In addition, since $\omega = 2\pi f$, the relation between frequency f and active power P can be described as a liner equation. For the same reason, the relation between reactive power Q and voltage error ΔV is also found. According to [Peas, 2006], [Kamel, 2013], [Tian, 2010], and [Banerji, 2013], f and V are described as follows:

$$f = f_0 - k_P \times P \tag{2.8}$$

$$V = V_0 - k_Q \times Q \tag{2.9}$$

where f_0 and V_0 are the idle values of the frequency and voltage (values of the frequency and terminal voltage at no load conditions), k_P and k_Q are the droop slopes (positive quantities). A droop control method can be shown in Figure 2.3. *f-P* droop character and *V-Q* droop character are the two parts of the droop control method.

(a) Frequency droop character   (b) Voltage droop character
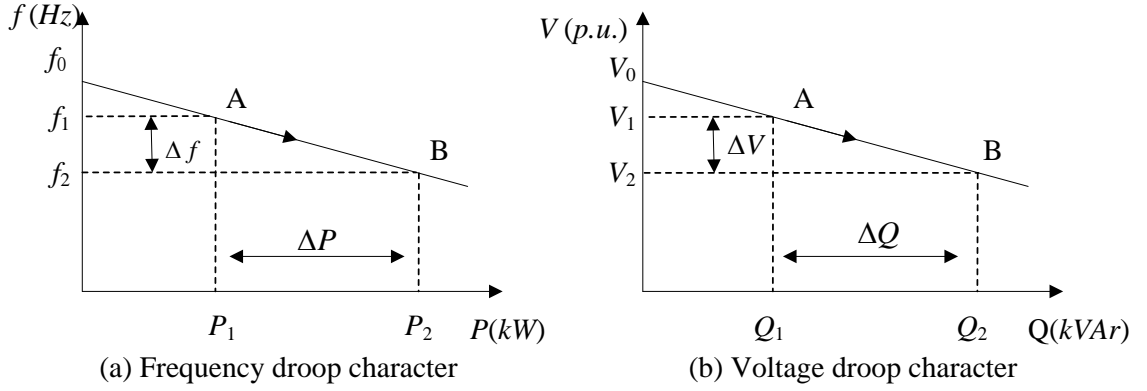
Figure 2.3 Droop control.

For example, when the demand for active power and reactive power increases, the operating point shifts from points A to B. It denotes that more active power and reactive power need to be generated by a DG.

Normally, a power system has a droop character. When the power sources cannot support the load demand, the frequency of the system tends to drop down. For the *f* droop character, when the frequency decreases, DGs need to generate more power to support the load demand. On the contrary, when the system frequency increases, DGs need to reduce the power generation to stabilize the system. Similarly, *V* droop character has the same

application to adjust reactive power Q. In the remaining work, only the relation between frequency f and active power P is to be discussed.

The advantages of the droop control method are as follows:

1. It can be widely used whenever the microgrid is worked as an islanded or grid-connected mode.
2. It can enable the sharing of the load among different DGs, which disperses the pressure of load demand to each DG and prevents any DGs from being overloaded.
3. It can be a part of a coordination control method, to be discussed later in this thesis, since it can work with other control methods well.

However, the droop control method has some disadvantages. Because there are not any reference frequency and voltage, the frequency and voltage are always changing. The system is difficult to be stabilized and often requires long time to achieve a desired stability level.

2.1.2 *P/Q* Control

When a *P/Q* control method is used, it aims to generate the constant values of active power and reactive power depending on the reference values. Its theory is shown in Figure 2.4.

(a) Frequency droop character   (b) Voltage droop character
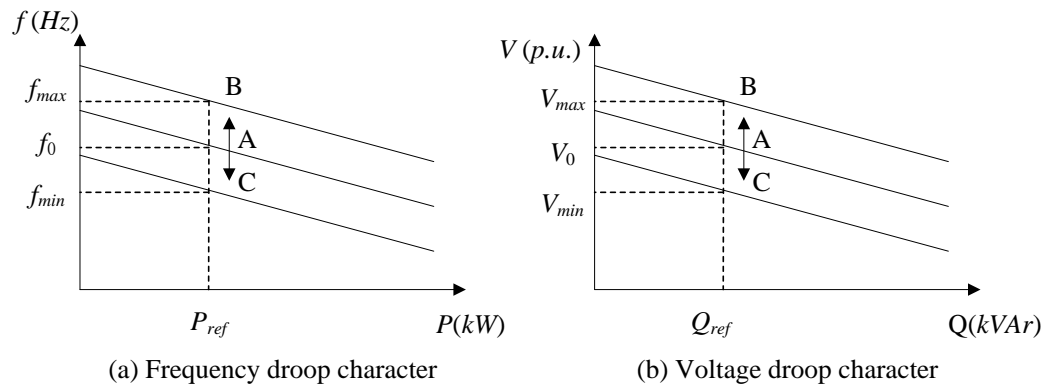
Figure 2.4 *P/Q* control.

It also depends on the frequency droop character and voltage droop character. However, it is different from the droop control. The curves of *f* and *V* in Fig. 2.4 are not always fixed. They can be shifted by some external factors, such as load. For example, as Figure 2.4 shows, at an initial state, the system works at point A with voltage magnitude V_0 and frequency f_0. At the same time, the DG generates active power and reactive power which are set as reference values P_{ref} and Q_{ref}. If the load demand increases, in order to maintain the constant power output, the frequency and voltage have to decrease. Then, the working point is shifted from points A to C. Meanwhile, the DG generates the same values of active power and reactive power as previous ones. On the contrary, if the load demand is decreased, the working point is shifted to point B. In addition, the *P/Q* control-based DG can generate constant power as P_{ref} and Q_{ref} in the permissible frequency range ($f_{min}{\leq}f{\leq}f_{max}$) and voltage range ($V_{min}{\leq}V{\leq}V_{max}$).

As mentioned above, the *P/Q* control method has received only limited adoption, because the *P/Q* controller has to follow the variant of the system frequency and voltage. It is impossible to adjust the system frequency and voltage with this method. In conclusion, the DG under *P/Q* control cannot run independently. It has to work in a grid-connected mode or work with other DGs [Barsali, 2002]. But its advantage lies in that the DG with such control method can generate the maximum power at anytime. If the DG is a renewable energy source such as a photovoltaic panel and wind turbine, the maximum power output is certainly desired as it belongs to the class of clean and green energy.

2.1.3 *V/f* Control

A *V/f* control method is similar to a *P/Q* control method, which satisfies *f* droop character and *V* droop character. But the difference between them is that the DG under the former

aims at generating constant voltage and constant frequency instead of constant active and reactive power in the latter [Tian, 2010]. The f and V-curves of the V/f control method are shown in Figure 2.5.

(a) Frequency droop character   (b) Voltage droop character
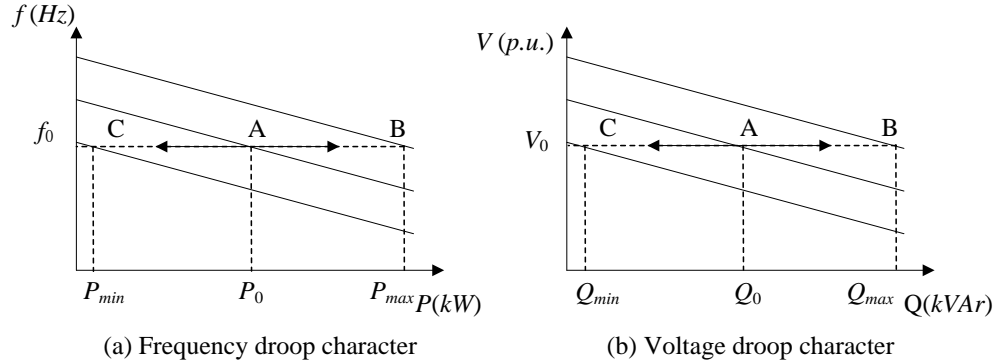
Figure 2.5 V/f control.

In Figure 2.5, when the system works at point A as an initial state, the DG needs to generate active power P_0 and reactive power Q_0. When the system requires different active and reactive power outputs, the f and V-curves are shifted upward or downward. For example, if the active power load demand increases, the system frequency decreases. To respond to the system frequency decrease, the f-curve is shifted upward. In order to maintain the constant frequency, the DG needs to generate more active power. The working point is shifted from points A to B. Similarly, if the reactive power demand is changed, the working point is shifted to respond to the variant reactive power load demand. In conclusion, the V/f control-based DG is able to generate the constant values of frequency and voltage in an allowed capacity range ($P_{min} \leq P \leq P_{max}$ and $Q_{min} \leq Q \leq Q_{max}$). Thus, it can be operated in an islanded mode independently. The DG with less external disturbance, such as diesel generator and hydroelectric generator, is easy to be controlled with the V/f control method.

2.2 Basic Coordination Control Methods

Comparing with a national grid or traditional defined power system, a microgrid is small. According to [Piagi, 2006] and [Dimeas, 2005], a microgrid is a "plug and play" system. Thus, it should be operated in both grid-connected and islanded modes. Proper coordination control not only needs to assist the microgrid to work in both modes, but also helps the microgrid switch from a mode to another smoothly. This study focuses on the coordination control in an islanded mode.

2.2.1 Master-slave Control

Under the master-slave control, one of the DGs should operate under the V/f control and generate constant voltage and frequency [Peas, 2005]. Such constant voltage and constant frequency provide reference values for other DGs. The DG that operates under the V/f control is called a master generator. Other DGs working as slave generators follow this master one to support the microgrid in an islanded mode. Under master-slave control, the master generator responds to the variant load demand; while other DGs are set to work under the P/Q control or droop control. In order to enable the master-slave control, the master generator is required to have relatively a large capacity. Therefore, it can respond to a variant load smoothly and swiftly. Its control mode can be switched to the V/f control mode from any others rapidly, during the islanding process of a microgrid.

The advantages of master-slave control are as follows:

1. The master generator can supply constant frequency and constant voltage for other DGs as reference values.
2. The entire system is relatively stable.

Its disadvantages of master-slave control are as follows:

1. Only one DG can be set to be a master generator.
2. High capacity requirement is posed to a master generator.

2.2.2 Point to Point Control

According to [Piagi, 2006], a point to point control mode is different from a master-slave control mode. All DGs under point to point control are the same. There is no distinction between the master and slave generators. The most popular control method is droop control. Every DG under the droop control shares the load demand and bears the variant system load. Meanwhile, every DG is engaged to adjust the system frequency and voltage. In another aspect, because all DGs are under the droop control, no DG needs to change the control mode during the islanding process.

The advantages of point to point control are as follows:

1. All DGs can share and bear the variant system load; and
2. It poses less requirement of DG than the master-slave control.

However, since a power system is dynamic, it is difficult for this control method to obtain proper reference values.

2.2.3 Hierarchical Control

Hierarchical control divides traditional control into several layers by means of a communication system. A common hierarchical control has two layers. The lower layer is a physical layer that contains DGs, monitors, load, etc. The higher one is called Microgrid Central Controller (MGCC) layer that contains load prediction, communication system, etc. MGCC, in this control mode, predicts the load demand and power generation of DGs [Xu, 2013]. After analyzing the system state, MGCC determines a schedule and sends the control signal to local controllers that belong to the physical layer. Meanwhile, the system

monitors at the physical layer and sends real time data to MGCC. Then MGCC analyzes

the data and adjusts the operation schedule again. MGCC can also detect and diagnose the

fault of the system to provide system protection.

CHAPTER 3

PETRI NET MODELING OF MICROGRIDS

3.1 Petri Nets

In [Lin, 2006], [Zhou, 1995] and [Zhou, 1998], a Petri net (PN) is described as a tuple *PN*

={*P*, *T*, *Pre*, *Post*, *M*}

where

1. $P = \{p_1, p_2, \ldots, p_n\}$ is a non-empty finite set of places.
2. $T = \{t_1, t_2, \ldots, t_n\}$ is also a non-empty finite set of transitions with P∩T=∅.
3. *Pre*: $P \times T \rightarrow \mathbf{N}$ is a mapping that assigns a weight to the arcs from place to transitions and **N** is the set of natural numbers.
4. *Post*: $P \times T \rightarrow \mathbf{N}$ is a mapping that assigns a weight to the arcs from transitions to places.
5. *M*: $P \rightarrow \mathbf{N}$ is a marking representing the number of tokens in places with M_0 denoting the initial marking.

The preset of transition *t* is the set of all input places to *t*, $^\bullet t = \{p: p \in P$ and *Pre*(*p*, *t*)>0}. The post of *t* is the set of all output places from *t*, $t^\bullet = \{p: p \in P$ and *Post*(*t*, *p*)>0}. Similarly, *p*'s preset $^\bullet p = \{t: t \in T$ and *Post*(*t*, *p*)>0} and postset $p^\bullet = \{t: t \in T$ and *Pre*(*p*, *t*)>0}.

Incidence matrix: *A=Post*－*Pre*, defines all possible interconnections between places and transitions except self-loops, i.e., 1) a place is an input and output one of a same transition and 2) a transition is an input and output one of a same place. Its dimension is $|P| \times |T|$.

Definition 1: A transition $t \in T$ in PN is enabled if $\forall p \in P$

$$M(p) \geq Pre(p, t) \tag{3.1}$$

A transition t_i's firing at M leads to a new marking M'

$$M' = M + A \cdot u \tag{3.2}$$

where M' and M are $m \times 1$ column vectors representing the new and current marking, repectively, m is the place count, u is an $n \times 1$ column vector having a single one at its j-th position representing transition t_j's firing, and n is the transition count.

3.2 Hybrid Petri Nets

A hybrid Petri net (HPN) is an extention of the above defined PN by introducing continuous transitions, places and markings containing real numbers. In [David, 1997], [Gao, 1999] and [Xu, 2005], it is a tuple $H = (PN, S)$ that satisfies the following conditions:

1. $PN=\{P, T, Pre, Post, M\}$.
2. $P=P_d \cup P_c$ is the set of discrete places and continuous places with $P_d \cap P_c = \emptyset$. $p_d \in P_d$ represents a discrete place and $p_c \in P_c$ represents a continuous place.
3. $T=T_d \cup T_c$ is the set of discrete transitions and continuous transitions with $T_d \cap T_c = \emptyset$. $t_d \in T_d$ represents a discrete transition and $t_c \in T_c$ represents a continuous transition.
4. S is the set of firing speeds and enabled time intervals associated with continuous transitions; for $t_j \in T_c$, $S(t_j) = (v_j, h)$, where $v_j, h \in \mathbf{R}$, v_j is the firing speed associated with transition t_j and h is an enabled time interval.

Definition 2: A continuous transition $t_j \in T_c$ is enabled if $\forall p \in P$

If $p_i \in {}^\circ t_j \cap P_d$, $M(p_i) \geq Pre(p_i, t_j)$; and

If $p_i \in {}^\circ t_j \cap P_c$, $M(p_i) \geq 0$.

The marking of a discrete place is a natural number, while the marking of a continuous place is a positive real number.

For transition $t_j \in T_d$, at the beginning of its firing, the marking becomes:

$$\forall p_i \in \text{}^{\circ}t_j \cap P_d : M'(p_i) = M(p_i) - Pre(p_i, t_j) \tag{3.3}$$

After delay d_j, the marking becomes:

$$\forall p_i \in t_j \text{}^{\circ} \cap P_d : M(p_i)' = M(p_i) + Post(p_i, t_j) \tag{3.4}$$

where d_j denotes the time delay for a timed transition t_j. An immediate transition t_j can be seen as timed transition $d_j=0$. Note that if p_i is an input and output place of t_j, its marking after firing t_j at M should be $M(p_i) - Pre(p_i, t_j) + Post(p_i, t_j)$.

For transition $t_j \in T_c$, we assume that the firing begins at time τ_s, and ends at time τ_s+h. h denotes an enabled time interval. At any time point τ, $\tau \in [\tau_s, \tau_s+h]$ the marking becomes:

$$\forall p_i \in \text{}^{\circ}t_j \cap P_c : M'(p_i) = M(p_i) - v_j(\tau) \cdot Pre(p_i, t_j) \cdot h \tag{3.5}$$

$$\forall p_i \in t_j \text{}^{\circ} \cap P_c : M'(p_i) = M(p_i) + v_j(\tau) \cdot Post(p_i, t_j) \cdot h \tag{3.6}$$

Note that if p_i is an input and output place of t_j, its marking after firing t_j at M should be $M(p_i) - v_j(\tau) Pre(p_i, t_j) h + v_j(\tau) Post(p_i, t_j) h$.

3.3 Finite Capacity Petri Nets

According to [Qiao, 2013], a finite capacity Petri net is a tuple *FC* = (*PN*, *C*) that satisfies

the following conditions:

1. *PN* is an ordinary Petri net, *PN*={*P*, *T*, *Pre*, *Post*, *M*};
2. *C: P*→$\mathbf{N}^+$ is a capacity function where *C*(p_i) represents the number of tokens that place p_i can hold at a time.

Definition 3: A transition $t_j \in T$ in PN is enabled if $\forall p_i \in P$:

$$M(p_i) \geq Pre(p_i, t_j) \tag{3.7}$$

and

$$C(p_i) \geq M(p_i) - Pre(p_i, t_j) + Post(p_i, t_j) \tag{3.8}$$

If a transition *t* is enabled, firing it at next *M* yields *M'* as follows:

$$M'(p_i) = M(p_i) - Pre(p_i, t_j) + Post(p_i, t_j) \tag{3.9}$$

Definition 3 indicates that t_j is enabled and can fire if there are enough tokens in all

places in $^\circ t_j$ and at the same time there are enough free spaces in all the places in $t_j ^\circ$. Thus,

t_j is enabled when these two conditions are both satisfied.

3.4 Power Systems Modeled with Petri Nets

3.4.1 Load Sharing Model

In [Chamorro, 2012], a load sharing model based on a PN is given. Its structure is shown in Figure 3.1. The meanings of places and transitions are listed in Table 3.1.

In this PN model, the coordination load sharing process is composed of multiple power converters and monitoring units that are in charge of informing the load thresholds and the turning on/off selection. The process of load sharing is described as follows:

A token in p_1 represents the start of the operation. This state indicates that there must be an initial power converter always on. In this model, unit1 is set to be the initial power converter. Then, t_1 is enabled to monitor the control action of the power converter giving the state of unit1. p_2 indicates the monitoring action of the load under the control action of the power converter unit1. t_2 specifies the threshold limit to be controlled by one unit only. Then, p_3 turns on the power converter unit2. In this stage, the process is repeated, checking the control state, monitoring the new load demand and observing the boundaries of deactivation or activation of the other power units.
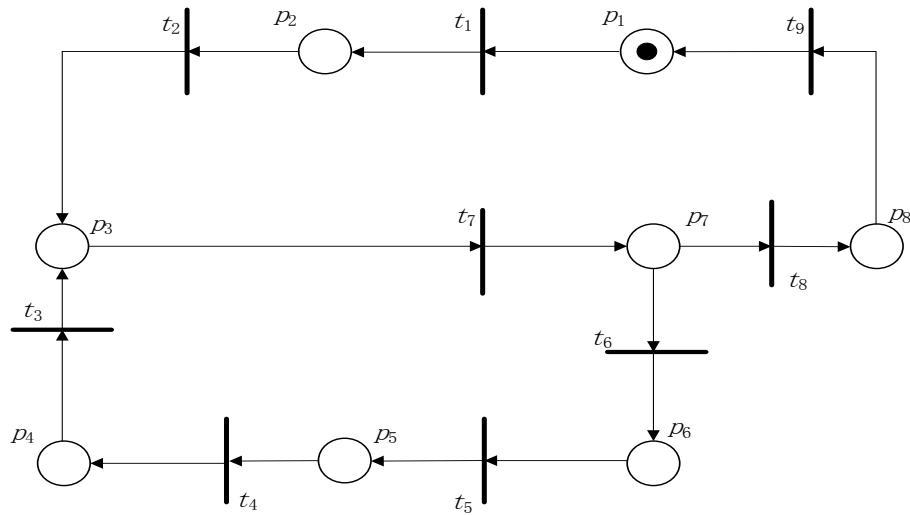
Figure 3.1 A load sharing PN model [Chamorro, 2012].

Table 3.1 Meanings of Places and Transitions of a Load Sharing PN Model

p	p_1	Unit1 on
	p_2	Load monitor1 on
	p_3	Unit2 on
	p_4	Unit3 off
	p_5	Load monitor3 on
	p_6	Unit3 on
	p_7	Load monitor2 on
	p_8	Unit2 off
t	t_1	Unit1 is ready
	t_2	Load reaches level 1
	t_3	Unit3 is turned off
	t_4	Load is below level 2
	t_5	Unit3 is ready
	t_6	Load reaches level 2
	t_7	Unit2 is ready
	t_8	Load is below level 1
	t_9	Unit1 is on

3.4.2 Wind Turbine Model

According to the speed of wind V, the energy produced by a wind turbine may follow different rules. The first mode is that if V is greater than the start-up speed V_a and smaller than the rated speed V_n, then the generation is proportional to the wind speed, $E_w = f(V)$. The second mode corresponds to the case where the wind speed is greater than V_n. Then the wind turbine generates at its maximum capacity, $E_w = E_{max}$. The third mode aims at the case when wind speed is less than start-up wind speed V_a. In this case, the power output of a turbine is 0 ($E_w = 0$). An HPN model is illustrated in Figure 3.2.

Discrete places p_1, p_2 and p_3 represent three operating modes of a wind turbine respectively. Continuous place p_0 represents the energy produced by the wind turbine. If p_1 holds a token, the first mode of the wind turbine is activated. This place controls the firing speed of transition t_1. Since the energy generated is proportional to the wind speed, the equation is described as $E_w=f(V)$. Therefore, t_1'sfiring speed is $v=f(V)$.

A token in p_2 activates the second mode, where the energy produced by the wind turbine is at its maximum capacity, i.e., $E_w=E_{max}$. Thus, the firing speed of continuous transition t_2 is $v=E_{max}$.
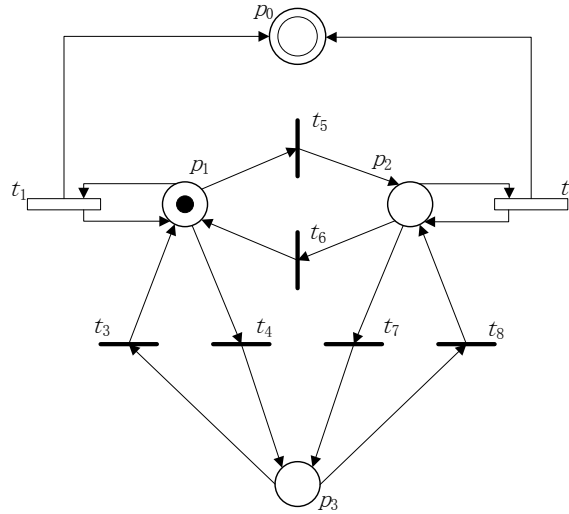
Figure 3.2 An HPN model of a wind turbine [Sava, 2014].

A token in place p_3 means that the third mode is active. At this mode, the wind turbine does not produce energy, and thus no token enters p_0.

The evolution from any mode to another is accomplished by firing transitions, t_3 - t_8. Under different environmental conditions, a different transition is enabled and fires. For instance, initially, the wind speed V is less than the rated wind speed V_n, but greater than the start-up speed V_a, then the wind turbine is operated at the first mode. If wind is now

stronger than before and the wind speed V is greater than V_n, transition t_5 is enabled, and the first mode is shifted to the second mode.

3.4.3 Photovoltaic Cell Model

The energy produced by a photovoltaic cell is related to the intensity of sunlight. It is denoted as E_p and the intensity of sunlight is denoted as H_t. The relation between E_p and H_t is $E_p = f_2(H_t)$ when the intensity of sunlight is greater than a threshold value H_{t0}. Otherwise, the photovoltaic cell does not produce energy, i.e., $Ep = 0$. An HPN model of a photovoltaic cell is shown in Figure 3.3.
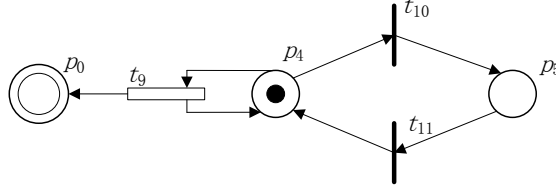
Figure 3.3 An HPN model of a photovoltaic cell [Sava, 2014].

The production of energy by a photovoltaic cell is modeled by continuous transition t_9. Its firing speed is defined as $v_9 = f_2(H_t)$. A token in place p_4 means that the sunlight is strong enough to produce energy, i.e., $H_t \geq H_{t0}$. Discrete place p_5 models the state of the photovoltaic cell with zero energy generation. Transitions t_{10} and t_{11} model the mode shifting. If $H_t < H_{t0}$, t_{10} is enabled and the token is added into p_5 which means that the cell cannot produce energy anymore. On the contrary, if $H_t \geq H_{t0}$, t_{11} is enabled and the token moves to p_4 to produce with firing speed $v_9 = f_2(H_t)$. Continuous place p_0 denotes the amount of produced energy that is not consumed.

3.4.4 Storage Battery Model

The storage device stores energy produced in order to respond to the shortage during high energy demand interval. There are three operating modes for a storage device: 1) charging; 2) storing; and 3) discharging. The HPN model of storage battery is illustrated in Figure 3.4.
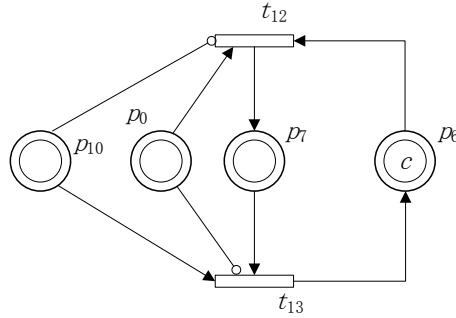
Figure 3.4 An HPN model of a storage battery [Sava, 2014].

Continuous place p_0 models the amount of energy produced by the system and not consumed yet. Continuous place p_{10} models the shortage of energy demand.

Continuous transition t_{12} models the charging of the battery with firing speed v_{12}. On the opposite, continuous transition t_{13} models the discharging of the battery with firing speed v_{13}. Continuous place p_7 models the amount of energy stored and p_6 models the storage capacity.

The input places of transition t_{12} are p_0, p_6 and p_{10}. p_{10} is connected to transition t_{12} via an inhibitor. This inhibitor indicates that if the battery is being charged, it represents that the system has enough energy to meet the energy demand, and the surplus energy is charged into battery. In a traditional PN, a transition which is connected to a discrete place via an inhibitor arc is disabled when $M(p) \geq 1$. However, in HPN, a transition which is connected to a continuous place via an inhibitor arc is disabled when $M(p) > 0$.

Consequently, the battery is at a charging mode when t_{12} is enabled if the amount of stored energy has not reached the capacity ($M(p_6)>0$), and the amount of produced energy exceeds the demand ($M(p_0)>0$ and $M(p_{10})=0$).

The input places of transition t_{13} are p_0, p_7 and p_{10}. Place p_0 is linked to t_{13} via an inhibitor. This inhibitor represents that the demand exceeds the production of energy and the battery is at a discharging mode. Thus, the battery is discharged if the amount of stored energy is positive ($M(p_7)>0$) and the demand is greater than the produced energy of system ($M(p_0)=0$ and $M(p_{10})>0$).

3.4.5 Diesel Generator Model

A diesel generator has two modes: 1) energy production mode and 2) non-production mode. An HPN model of a diesel generator is depicted in Figure 3.5.
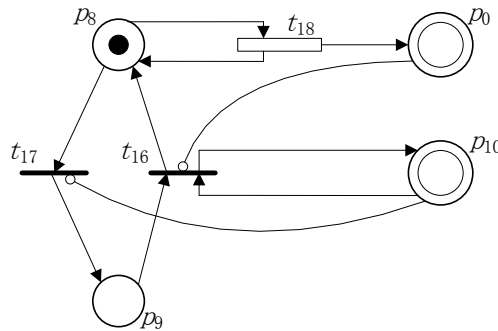
Figure 3.5 An HPN model of a diesel generator [Sava, 2014].

A token in place p_8 models the energy production mode. A token in p_9 marks the non-production mode. Energy production is modeled by firing the continuous transition t_{18} depending on a specific firing speed v_{18}. The energy production is triggered by firing transition t_{16} when the demand is not satisfied ($M(p_{10})>0$) and there is no available energy left ($M(p_0)=0$). The diesel generator switches to the non-production mode when energy

demand is satisfied ($M(p_{10}=0)$). Place p_0 is linked to t_{16} via an inhibitor, which means that the system has enough energy and the diesel generator is not needed to produce energy. There is no need to switch a non-production mode to a production mode ($M(p_0>0)$).

3.4.6 On-load Tap Changing Model

According to [Paruchuri, 2005], a PN model can be used to simulate an On-Load Tap Changing (OLTC) transformer as shown in Figure 3.6. The meanings of places and transitions of an OLTC transformer model are listed in Table 3.2.
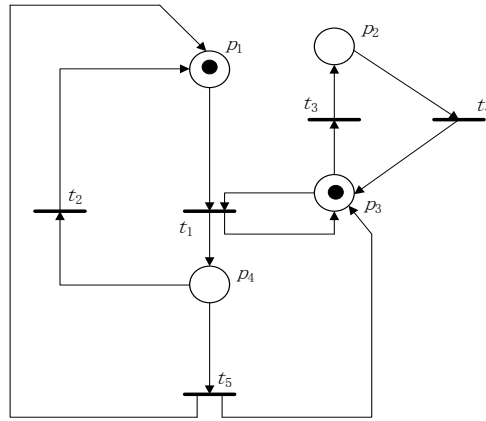
Figure 3.6 A PN model of an OLTC transformer [Paruchuri, 2005].

Table 3.2 Meanings of Places and Transitions of an OLTC Transformer Model

p	p_1	Voltage acceptable
	p_2	Tap at max
	p_3	Tap position available
	p_4	Timer is active
t	t_1	Voltage falls
	t_2	Voltage recovers
	t_3	Tap reaches max
	t_4	Tap position decreases
	t_5	Timer reaches a pre-set time

Tap changing is one of the ways to adjust a system voltage. When the voltage falls below an acceptable voltage level and the tap position is available to adjust, t_1 is fired and a token moves from p_1 to p_4, which means that the timer is activated. When timer reaches a pre-set time, one token is moved into p_3 to describe that the tap position is adjusted. If t_3 is enabled, one token is held in p_2, meaning that the tap is at maximum and cannot be changed any more. Once the voltage is recovered, the token moves back to the p_1 and t_4 can be enabled to move a token back to p_3 that shows the tap of the transformer can be adjusted again.

3.4.7 An HPN Model of a 4-DG Microgrid

A microgrid is often composed of a load, a battery system and multiple DGs. In Figure 3.7, it is a 4-DG microgrid. There are a wind turbine, photovoltaic cell, diesel generator, battery and load. All of them are connected to the Bus directly.
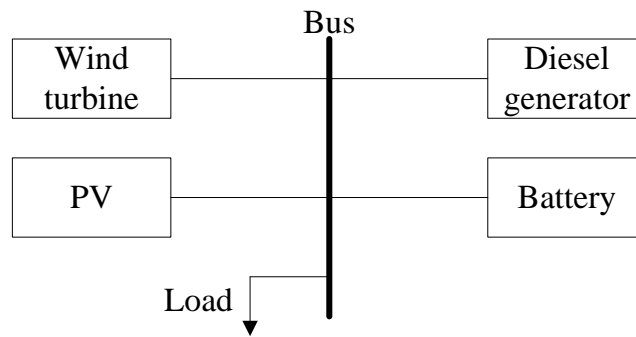
Figure 3.7 A 4-DG microgrid.

In Figure 3.8, it is an HPN model of a 4-DG microgrid. The wind turbine, battery, photovoltaic cell, and diesel generator are represented by four dotted boxes in it.

Figure 3.8 An HPN model of a 4-DG microgrid.

The wind turbine has places, p_1-p_3, and transitions, t_1-t_8. According to the wind speed V, the wind turbine has three operating modes. It is operated under the first mode if V is greater than the start-up speed V_a but smaller than the rated speed V_n. At this mode continuous transition t_1 is enabled with the firing speed v_1 ($v_1 = E_w = f(V)$). However, if the wind speed is greater than V_n, t_2 is enabled with the firing speed v_2 ($v_2 = E_w = E_{max}$) and the

system runs at the second mode. The third one aims at the case when the wind speed is less than the start-up wind speed V_a. In this case, the power output of the wind turbine is 0 (E_w=0). The photovoltaic cell has places, p_4-p_5, and transitions, t_9-t_{11}. It has two operating modes, either on or off. The firing speed of t_9 is v_9, depending on the intensity of sunlight when the photovoltaic cell is on. The power output of this photovoltaic cell is zero when it is off. The firing speed v_{wp} represents the rate of energy produced by both wind turbine and photovoltaic cell. Clearly, $v_{wp}=v_1+v_9$ or $v_{wp}=v_2+v_9$, when the wind turbine is operated at the first or second mode. The battery model is composed of places, p_6-p_7, and transitions, t_{12}-t_{13}. It has three operating modes, charging, storing and discharging. The firing speed v_{12} is associated with t_{12}, when it is operated at the charging mode. On the contrary, the firing speed v_{13} is associated with t_{13}, when it is in the discharging one. For the diesel generator, its HPN module consists of places, p_8-p_9, and transitions, t_{14}-t_{16}, with two operating modes, energy production and non-production mode. When it is on, p_8 holds a token. Then t_{14} is triggered with the firing speed v_{14}. p_0 denotes the energy produced by both wind turbine and photovoltaic cell. When the system has surplus energy and can meet the load, $M(p_0)>0$; otherwise $M(p_0)=0$. p_{10} represents the shortage of energy demand. When the system does not have enough energy, $M(p_{10})>0$; otherwise $M(p_{10})=0$. Meanwhile, t_{load} represents the load demand with the firing speed v_{load}. t_0 means that the wind turbine and photovoltaic cell respond to the load demand with the firing speed v_0 and $v_0=min(v_{wp}, v_{load})$. ε in Figure 3.8 is a small quantity set to be the minimum energy unit. This arc with ε as its weight is required in order to detect if its connected continuous place has any energy in it.

Table 3.3 Meanings of Places and Transitions of the HPN Model of a 4-DG Microgrid

p_d	p_1	The first mode of wind turbine
	p_2	The second mode of wind turbine
	p_3	The third mode of wind turbine
	p_4	The photovoltaic cell on
	p_5	The photovoltaic cell off
	p_8	The diesel generator on
	p_9	The diesel generator off
p_c	p_0	The energy produced by both wind turbine and photovoltaic cell
	p_6	The storage capacity of the battery
	p_7	The amount of energy stored in the battery
	p_{10}	The shortage of energy demand
t_d	t_3	The wind turbine switches from the first mode to the third one.
	t_4	The wind turbine switches from the third mode to the first one.
	t_5	The wind turbine switches from the first mode to the second one.
	t_6	The wind turbine switches from the second mode to the first one.
	t_7	The wind turbine switches from the third mode to the second one.
	t_8	The wind turbine switches from the second mode to the third one.
	t_{10}	The photovoltaic cell on
	t_{11}	The photovoltaic cell off
	t_{15}	The diesel generator off
	t_{16}	The diesel generator on
t_c	t_0	Both wind turbine and photovoltaic cell respond to the load demand.
	t_1	The energy produced by the wind turbine at the first mode
	t_2	The energy produced by the wind turbine at the second mode
	t_9	The energy produced by the photovoltaic cell
	t_{12}	The charging of the battery
	t_{13}	The discharging of the battery
	t_{14}	The energy produced by the diesel generator
	t_{load}	Load demand

There are three circumstances for this 4-DG microgrid. For the first circumstance, the energy produced by the wind turbine and photovoltaic cell cannot meet the load demand ($v_{load}>v_{wp}$). Then $M(p_0)=0$ and $M(p_{10})>0$. In order to compensate the shortage of load demand, the diesel generator is operated in its production mode by holding a token in p_8. Meanwhile, the battery is switched to the discharging mode to release its energy. For the second circumstance, the energy produced by the wind turbine and photovoltaic cell is equal to the load demand ($v_{load}=v_{wp}$). Thus $M(p_0)=0$ and $M(p_{10})=0$. In this case, the battery is in the storing mode and the diesel generator generates power with its minimum capacity. When the wind turbine and photovoltaic cell can generate enough energy and the microgrid has surplus energy, the system is at the third circumstance. In this circumstance, $v_{load}<v_{wp}$, and thus $M(p_0)>0$ and $M(p_{10})=0$. t_{15} is enabled, and the token goes to p_9 from p_8, which means that the diesel generator is turned off. The battery is switched to the charging mode by triggering t_{12}, and charged with the firing speed v_{12}.

In a real microgrid, an example curve of daily load demand is shown in Figure 3.9. The curve of daily energy produced by the wind turbine is shown as an example in Figure 3.10. The maximum capacity of the wind turbine is 2 *kw*. v_w represents the rate of daily energy produced by the wind turbine. Obviously, $v_w=v_1$ or $v_w=v_2$, when the wind turbine is operated at the first or second mode. The curve of daily energy produced by the photovoltaic cell is described as an example in Figure 3.11. All example curves are piecewise constant.

A reachability graph is shown in Figure 3.12. $\Delta\tau$ is a short time interval that is a short period of time when the battery and the diesel generator are required to start or to generate power or stop. ε is a minimum energy unit that is the amount of the shortage of

energy or the stored energy in a short time interval $\Delta\tau$. Meanwhile, $\tau+\Delta\tau$ represents a short time after time point τ. For example, $8+\Delta\tau$ denotes a moment right after 8 o'clock. The firing speed vector $v=(v_0, v_1, v_2, v_9, v_{12}, v_{13}, v_{14}, v_{load})$ is associated with the continuous transitions and is constant during the enabling time interval.
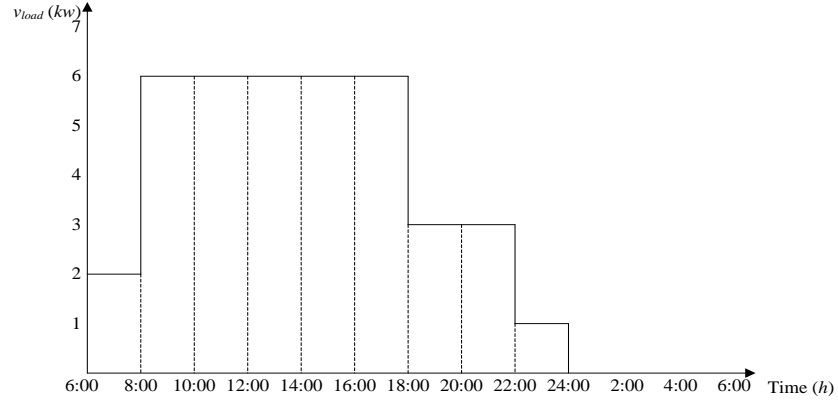
Figure 3.9 An example curve of daily load demand.
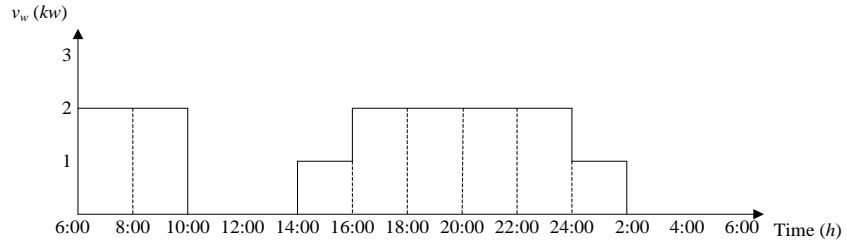
Figure 3.10 An example curve of daily energy produced by the wind turbine.
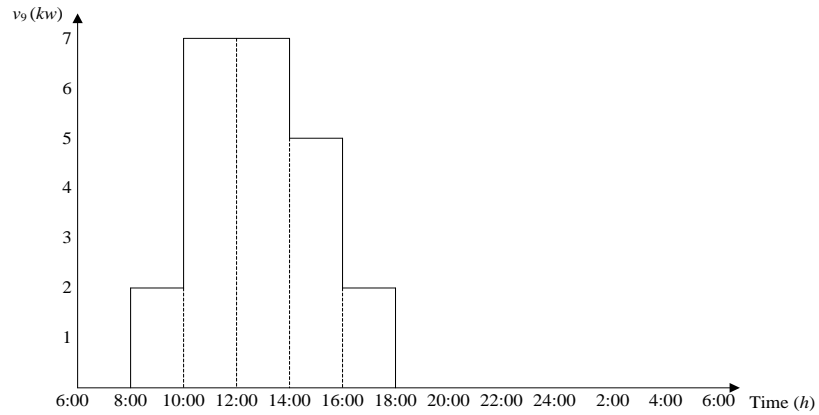
Figure 3.11 An example curve of daily energy produced by the photovoltaic cell.

$$\tau=6 \quad (0\ 0\ 0\ 1\ 0\ 1\ 2\ 8\ 0\ 1\ 0)$$

$$t_7 \downarrow$$

$$\tau=6 \quad (0\ 0\ 1\ 0\ 0\ 1\ 2\ 8\ 0\ 1\ 0)$$

$$v_{wp}=v_{load} \downarrow v=(2\ 0\ 2\ 0\ 0\ 0\ 0\ 2)$$

$$\tau=8 \quad (0\ 0\ 1\ 0\ 0\ 1\ 2\ 8\ 0\ 1\ 0)$$

$$t_{11} \downarrow$$

$$\tau=8 \quad (0\ 0\ 1\ 0\ 1\ 0\ 2\ 8\ 0\ 1\ 0)$$

$$v_{wp}<v_{load} \downarrow v=(4\ 0\ 2\ 2\ 0\ 0\ 0\ 6)$$

$$\tau=8+\Delta\tau \quad (0\ 0\ 1\ 0\ 1\ 0\ 2\ 8\ 0\ 1\ \varepsilon)$$

$$t_{16} \downarrow$$

$$\tau=8+\Delta\tau \quad (0\ 0\ 1\ 0\ 1\ 0\ 2\ 8\ 1\ 0\ \varepsilon)$$

Figure 3.12 Reachability graph of an HPN model of a 4-DG microgrid.

The initial marking is (0 0 0 1 0 1 2 8 0 1 0), which means that the wind turbine is operated at the third mode, both photovoltaic cell and diesel generator are off and the energy stored in the battery is 8 *kwh*. At 6 o'clock, since the wind speed is strong enough, the wind turbine switches from the third mode to the second one by moving a token from p_3 to p_2. However, the intensity of sunlight is not that strong, and thus the photovoltaic cell is off by holding a token in $p_5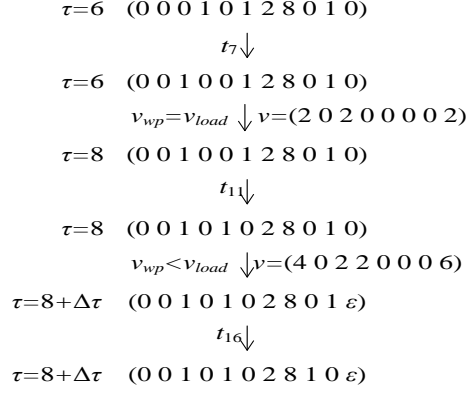$. Meanwhile, the energy produced by the wind turbine can meet the load demand. Thus, the firing speed vector is (2 0 2 0 0 0 0 2) during the period of time from 6 o'clock to 8 o'clock. At $\tau=8$, the marking is (0 0 1 0 0 1 2 8 0 1 0). At this time, since the intensity of sunlight is strong enough, t_{11} is enabled and a token goes to p_4 from p_5, which denotes that the photovoltaic cell is on. Then, continuous transition t_9 is enabled with the firing speed v_9=2 *kw*. According to the curve of daily load demand, the load demand increases to 6 *kw* at the same time. Then, the firing speed vector changes to (4 0 2 2 0 1 1 6). Since the wind turbine and photovoltaic cell cannot support the load demand, after a short time interval $\Delta\tau$, the value of p_{10} increases to ε and t_{16} is enabled which means that the diesel generator is turned on by moving a token from p_9 to p_8.

CHAPTER 4

COORDINATION CONTROL IN MICROGRIDS

In Chapter 2, various basic control methods and multiple coordination control methods are presented. Their advantages and disadvantages are discussed and compared. A coordination control method named multi-V/f control is given in [Zhang, 2014]. In this chapter, according to [Zhou, 1993] and [Hruz, 2007], a PN model is proposed and used to control multiple DGs and compared with multi-V/f control. Because f and V droop characters enjoy the same analysis method, the following sections discuss the f droop character only.

4.1 Multi-*V/f* Control

4.1.1 Concept of Multi-*V/f* Control

As a basic V/f control method and master-slave control, V/f control is adopted since V/f is able to supply stable reference values of system frequency and voltage. Due to this property, multi-V/f control can be used to control a system.

According to [Zhang, 2014], a coordination control rule is presented to regulate the system. On the basis of system frequency variation, only one of the DGs is operated as a master generator at a corresponding value of frequency. At each frequency level, the corresponding DG generates proper active power and reactive power to satisfy the load

demand. At the same time, other DGs are under P/Q control or droop control to generate their proper power. The multi-V/f control rule is shown in Figure 4.1.
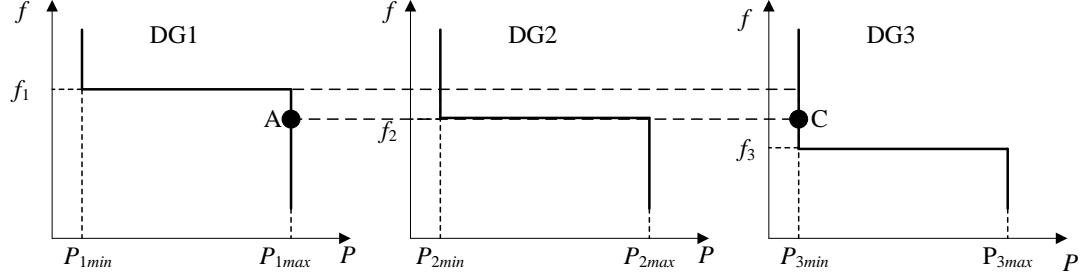
Figure 4.1 Multi-V/f control.

In Figure 4.1, three DGs are assumed under V/f control and values of reference frequency are f_1, f_2 and f_3. Initially, DG2 maintains the system frequency at f_2 as the master generator. DG1 and DG3 are under P/Q control. DG1 generates P_{1max} at point A and DG3 generates P_{3min} at point C. Following the increment of load, DG2 responds to the increment and generates more power in the range of its capacity. After DG2 reaches its maximum capacity, the system frequency decreases. If the system frequency decreases to f_3, the master generator shifts from DG2 to DG3. Then, DG2 is operated under P/Q control to generate P_{2max} and DG3 is operated under V/f control to respond the load demand variation.

The advantages of multi-V/f control are as follows:

1. More DGs can be operated as a master generator; and
2. The system is relatively stable.

Its disadvantages include:

1. It is hard to maintain the system at a stable state for a long time; and

2. Frequency must be changed to shift the master generator to another DG. The master generator is shifted to another DG depending on the system frequency variation.

4.1.2 An Example Based on Multi-V/f Control

A microgrid is assumed to have three DGs. DG3 is operated under droop control all the time. DG1 or DG2 is operated under V/f control when it is set to be a master generator, and is operated under P/Q control when it is not. All parameters of DGs are set in Table 4.1.

Table 4.1 Parameters of DGs

DG1	P_{min}=10kW, P_{max}=100kW, f_1=50.1Hz
DG2	P_{min}=20kW, P_{max}=150kW, f_2=50Hz
DG3	Droop slope k_P= -1/150 (Hz/kW)

Figure 4.2 shows the coordination control rules. DG1 is under V/f control if f_1=50.1Hz, while under P/Q control if $f_1 \neq$50.1Hz. DG2 is under V/f control if f_2=50Hz and under P/Q control if $f_2 \neq$50.1Hz. The load demand is shown in Figure 4.3. The system frequency is shown in Figure 4.4. The corresponding power outputs of DGs are shown in Figure 4.5.
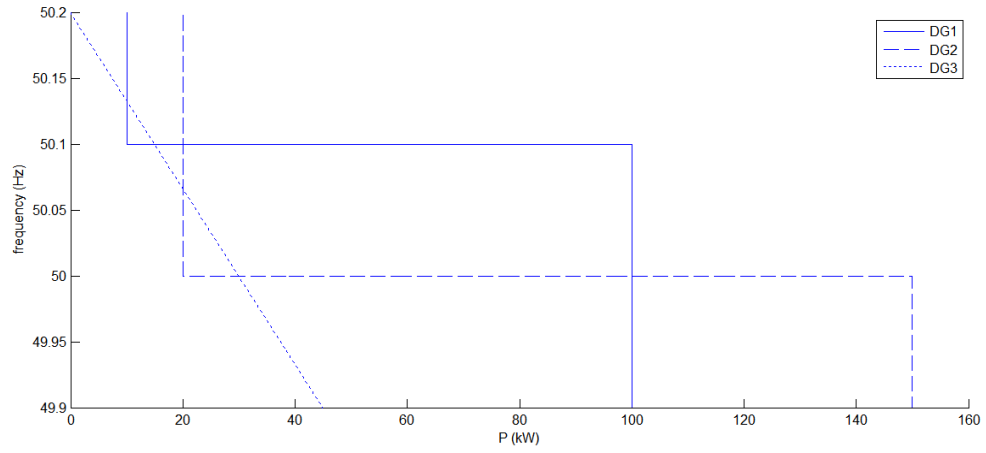
Figure 4.2 Multi-*V/f* control for a 3-DG system.
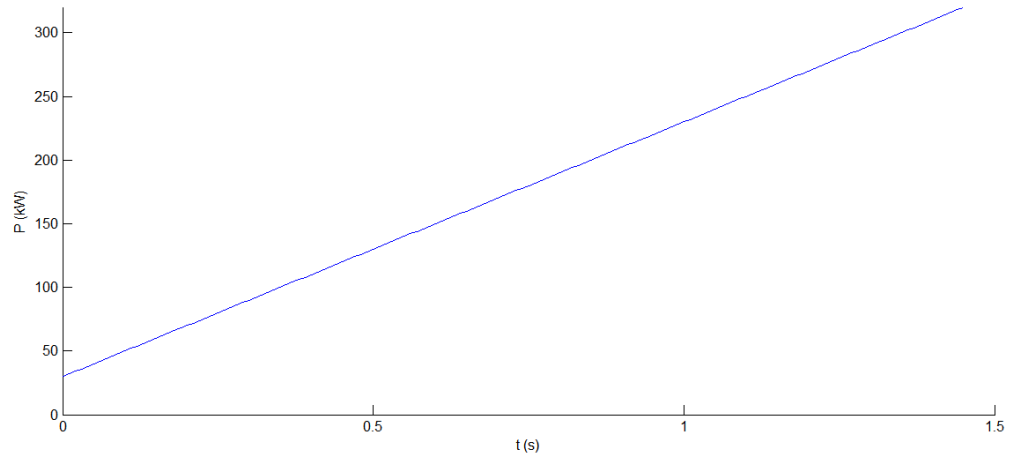
Figure 4.3 Load demand for a 3-DG system.
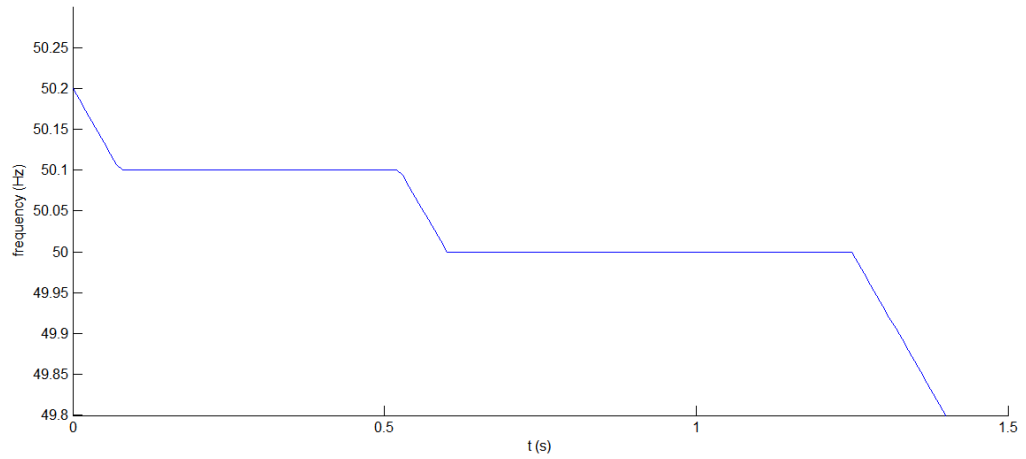
Figure 4.4 The simulation result of the system frequency based on the multi-*V/f* control.
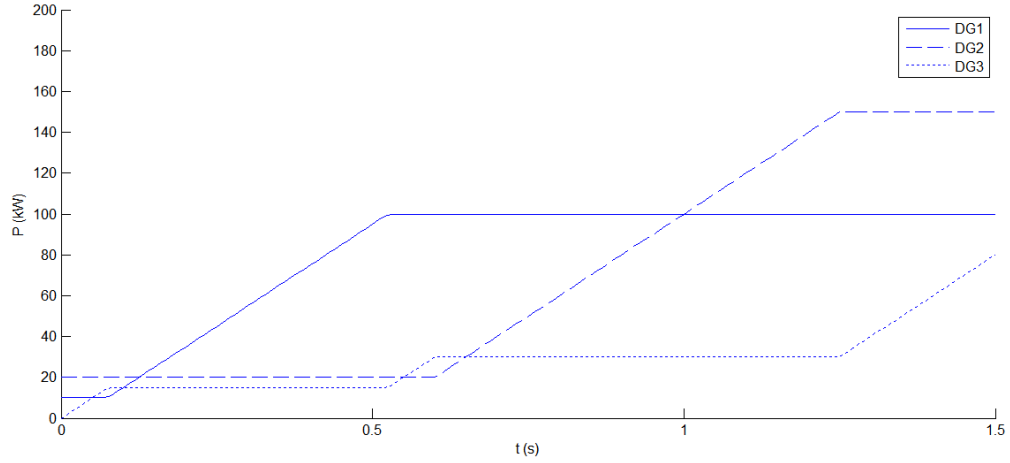
Figure 4.5 Power outputs of DGs based on the multi-*V/f* control.

Initially, at $\tau=0s$. The load is 30*kW*. The power generated by DG1, DG2 and DG3 is 10*kW*, 20*kW*, and 0*kW*, respectively. The system frequency decreases as the load increases. When it reaches 50.1*Hz*, DG1 is shifted to be a master generator. When DG1 reaches its maximum capacity, the system frequency decreases again to 50*Hz*. Then DG2 is operated as a master generator. From Figure 4.4, a stair-step shape is shown. The system frequency is stable at *f*=50.1*Hz* and *f*=50*Hz*. The time span is 0.65*s*, where *f=50Hz*.

4.2 Proposed Control Model Based on Petri Net

4.2.1 Coordination Control Based on Proposed PN Model

A 3-DG microgrid system can be described by using three operating modes: 1) When DG1 is a master generator under *V/f* control, DG2 is under *P/Q* control and DG3 under droop control; 2) When DG2 is a master generator under *V/f* control, DG1 is under *P/Q* control

and DG3 is under droop control; and 3) When DG3 is a master generator under droop, DG1 and DG2 are operated under *P/Q* control.

The PN is shown in Figure 4.6. In the middle of the PN model, there is a coordination control component. It contains places, p_1-p_3, and transitions, t_1-t_6, and models the mode switching. A token in p_1 marks the activation of the first mode. A token in p_2 marks the activation of the second one. Similarly, a token in p_3 marks the activation of the third one. Other three dotted boxes represent a system frequency detector, DG1 state detector and DG2 state detector, respectively. Places, p_4-p_7, and transitions, t_7-t_9, constitute the DG1 state detector that checks the state of DG1. Places, p_8-p_9, and transitions, t_{10}-t_{11}, constitute the DG2 state detector that checks the state of DG2. The system frequency detector has places, p_{10}-p_{13}, and transitions, t_{12}-t_{14}. It monitors the system frequency. The process of a 3-DG system based on the proposed PN model is shown as follows:

Initially, p_3 holds a token, which means that the system is operated at the third mode. The DG1 and DG2 state detectors check their states by holding tokens in p_4 and p_8. Besides, the system frequency is monitored by its detector by holding a token in p_{10}. Thus, the initial marking is [0 0 1 1 0 0 0 1 0 1 0 0 0]. When the system frequency detector finds that the system frequency approaches 50*Hz*, t_{13} is enabled and a token goes to p_{12} from p_{10}. Meanwhile, when the DG1 state detector finds that DG1 generates the power at its minimum capacity, t_7 is enabled and a token goes to p_5 from p_4. When p_3, p_5 and p_{12} have their tokens, t_1 is enabled. Then, a token goes to p_1 from p_3, which means that the master

41

generator is shifted from DG3 to DG1, and that the mode is switched from the third mode to the first one. At the same time, a token goes back to p_4 from p_5 and a token goes back to p_{10} from p_{12}. p_1 is connected to t_{13} via an inhibitor arc. It means that when the system is operated at the first mode, DG1 can provide a constant system frequency (f=50Hz). The system frequency detector does not need to monitor the system frequency. Similarly, when the system is operated at the first mode, DG1 generates the power in its allowed capacity range as the master generator. DG1 state detector just needs to check the state that DG1 reaches its maximum capacity. Thus, t_7 and t_9 are connected to p_1 via inhibitor arcs. Similarly, p_2 is connected to t_8, t_{11} and t_{13} via inhibitor arcs. p_3 is connected to t_{12} and t_{14} via inhibitor arcs. Under different system conditions, different transitions, t_7-t_{14}, are enabled. When the condition of mode switching is satisfied, the evolution from a mode to another is accomplished by firing transitions, t_1-t_6. In this stage, the process is repeated by monitoring the system frequency and checking the states of DG1 and DG2. Then, the system operating mode is switched from one mode to another.
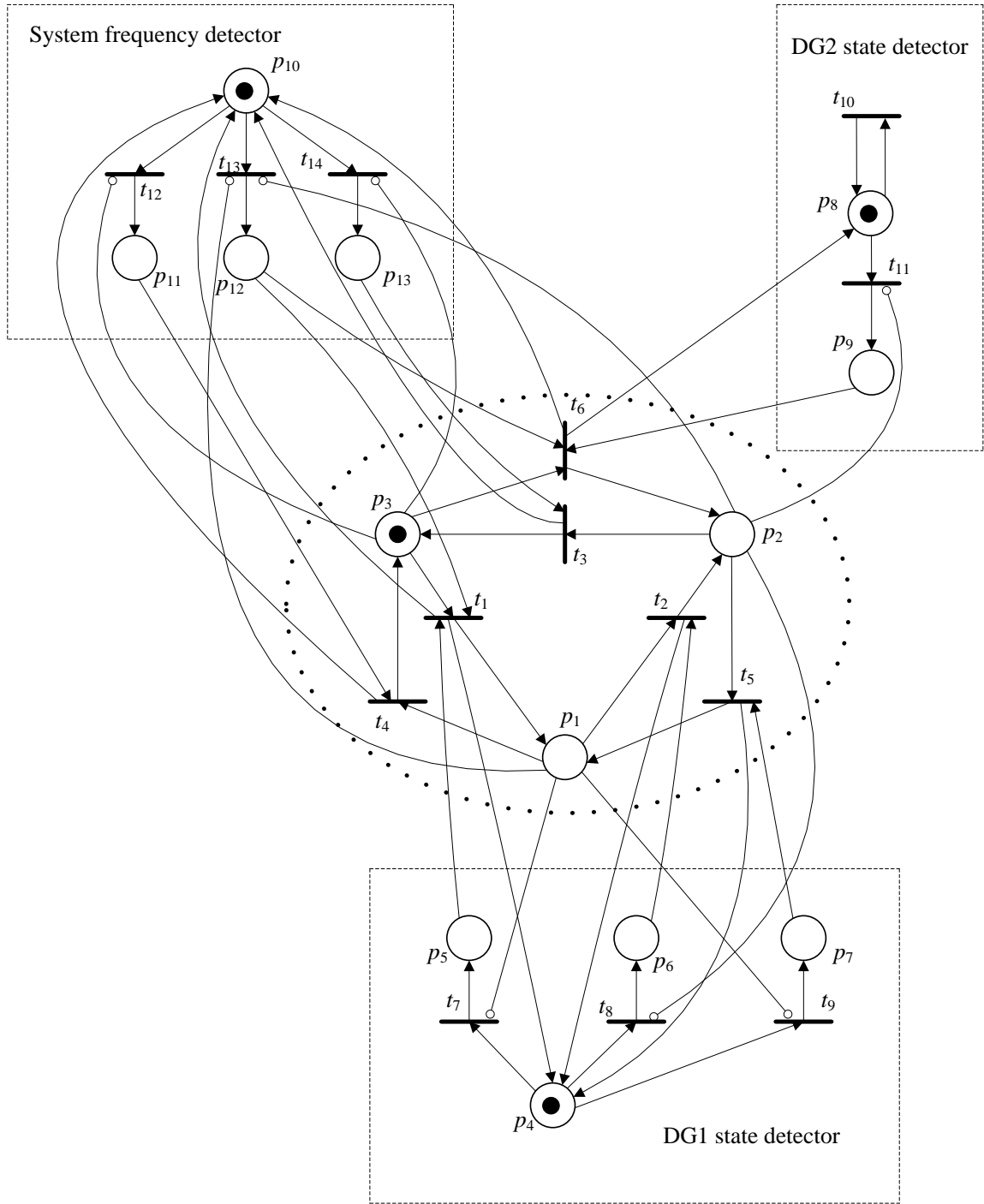
Figure 4.6 Proposed PN model for a 3-DG system.

Table 4.2 Meanings of Places and Transitions of the Proposed PN Model

p	p_1	The master generator is DG1
	p_2	The master generator is DG2
	p_3	The master generator is DG3
	p_4	Check the power output of DG1 (DG1 state detector)
	p_5	DG1 reaches its minimum capacity ($P_1=P_{1min}$)
	p_6	DG1 reaches its maximum capacity ($P_1=P_{1max}$)
	p_7	DG1 generates the power in its allowed capacity range ($P_{1min}<P_1<P_{1max}$)
	p_8	Check the power output of DG2 (DG2 state detector)
	p_9	DG2 generates the power in its allowed capacity range ($P_{2min}<P_2<P_{2max}$)
	p_{10}	Monitor system frequency (system frequency detector)
	p_{11}	$f > 50Hz$
	p_{12}	$f = 50Hz$
	p_{13}	$f < 50Hz$
t	t_1	The master generator shifts from DG3 to DG1
	t_2	The master generator shifts from DG1 to DG2
	t_3	The master generator shifts from DG2 to DG3
	t_4	The master generator shifts from DG1 to DG3
	t_5	The master generator shifts from DG2 to DG1
	t_6	The master generator shifts from DG3 to DG2

Enabling conditions of transitions, t_7-t_{14}:

t_7 is enabled when DG1 reaches its minimum capacity ($P_1=P_{1min}$).

t_8 is enabled when DG1 reaches its maximum capacity ($P_1=P_{1max}$).

t_9 is enabled when DG1 generates the power in its allowed capacity range ($P_{1min}<P_1<P_{1max}$).

t_{10} is enabled when DG2 reaches its minimum capacity ($P_2=P_{2min}$) or maximum capacity ($P_2=P_{2max}$).

t_{11} is enabled when DG2 generates the power in its allowed capacity range ($P_{2min}<P_2<P_{2max}$).

t_{12} is enabled when the system frequency is greater than $50Hz$ ($f > 50\ Hz$).

t_{13} is enabled when the system frequency equals $50Hz$ ($f = 50\ Hz$).

t_{14} is enabled when the system frequency is less than $50Hz$ ($f < 50\ Hz$).

According to [Zhou, 2005] and [Li, 2009], the reachability graph of the proposed PN model is shown in Figure 4.7. Every marking can be reached. Every transition can be enabled. All markings can go back to the initial marking. In addition, the maximum number of tokens in every place is 1. Thus, the whole PN model is live, reversible and safe.

Figure 4.7 Reachability graph of a PN model for a 3-DG system.

4.2.2 Simulation Result Based on the Proposed PN Model

This proposed PN model sets the same parameters as shown in Table 4.1. The result of

simulation is drawn in Figures 4.8 and 4.9.
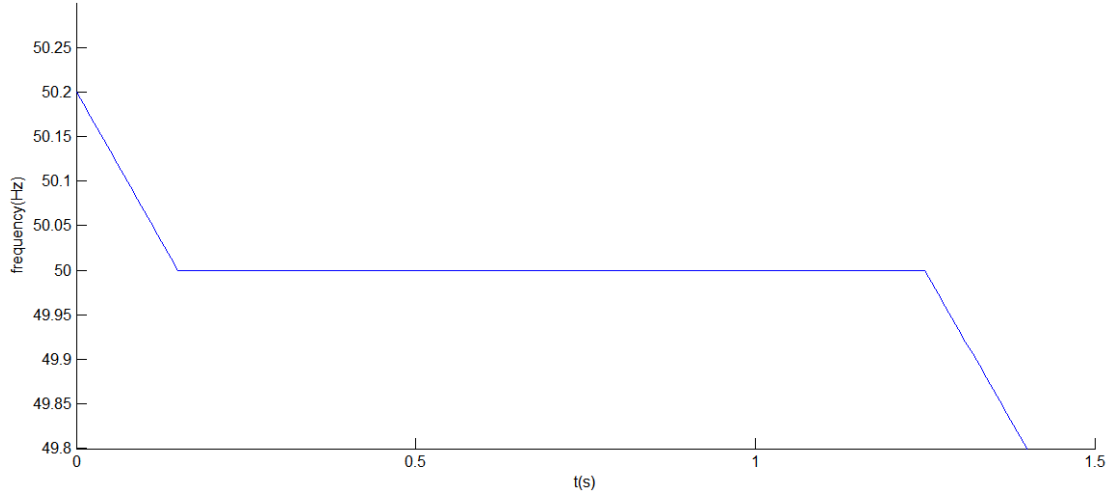
Figure 4.8 The simulation result of the system frequency based on the PN model.
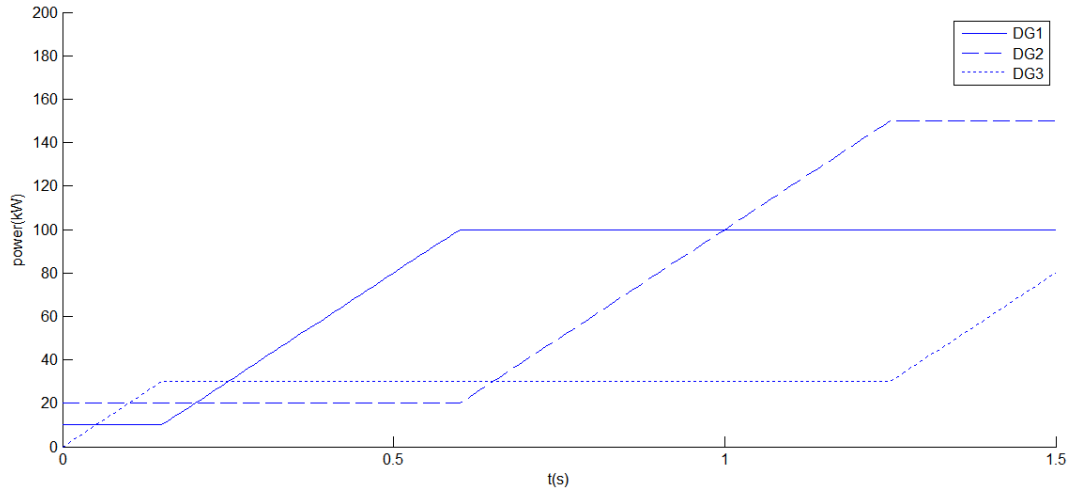
Figure 4.9 Power outputs of DGs based on the PN model.

By comparing Figure 4.8 with Figure 4.4, the system frequency is found to be stable in a long time interval. The stable time interval is from $\tau = 0.16s$ to $\tau = 1.26s$. The time span is $1.1s$ which is $0.45s$ longer than the time span in Figure 4.4. In addition, there is no stair-step shape of frequency, which denotes that the system is more stable than multi-V/f controlled system.

CHAPTER 5

HYBRID PETRI NET MODELS OF A MICROGRID

In a power system, large disturbance behavior is often described as complex interactions between continuous dynamics and discrete events. Components, such as generators and load, drive continuous system behaviors. Other components, such as a circuit breaker triggering, yield discrete events. It is challenging to model and analyze a power system, since it is a hybrid system that contains both continuous and discrete-event behavior. [Zhao, 2006] and [Hiskens, 2000] give a mathematic definition of an event and propose an algebraic method to model it. An On-Load Tap Changing (OLTC) transformer system is a complex system of this kind. At the beginning of this chapter, the algebraic method is used to describe this system. Then, an HPN method is proposed to model it. Finally, a comparison is given to show the differences between the algebraic method and the HPN method.

5.1 On-load Tap Changing Systems

In a microgrid, an OLTC system is a hybrid system shown in Figure 5.1. It consists of a generator, a transformer and two buses. Bus1 is connected to the generator, and thus its voltage equals to the terminal voltage of the generator. Bus2 is connected to the load with its voltage changing according to the load demand.

In this system, if the load decreases (increases), Bus2 voltage is increased (decreased). Corresponding to this situation, the transformer needs to shift the current tap position to a lower (upper) one to reduce (increase) Bus2 voltage. Voltage variant is a continuous behavior in a power system. However, the change of the tap position from one to another is a discrete event.
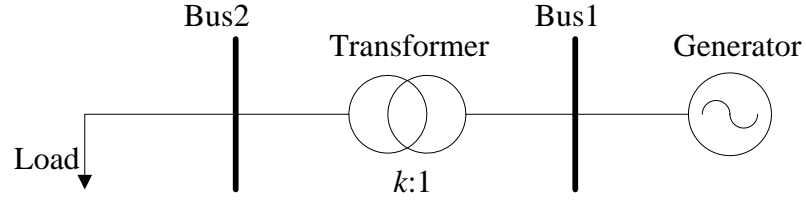
Figure 5.1 An OLTC system.

In an ideal model, the relation between Bus1 voltage (V_1) and Bus2 voltage (V_2) is defined as:

$$\frac{V_1}{V_2} = \frac{1}{k} \tag{5.1}$$

where k represents the current tap ratio. k^+ denotes the tap ratio after event occurs. $\Delta k = |k^+ - k|$ denotes that the tap ratio changes from the current one to a new one after an event occurs. It is set as 5% ($\Delta k = 0.05$) which denotes that every tap position change adjusts 5% of the primary side voltage. Thus, if the error between the actual voltage and the rate

voltage ($\Delta V = V_{actual} - V_{rate}$) is greater than 0.05 $p.u$, the tap needs to be changed once. The

rate voltage is assumed to be 1 $p.u$. We assume that Bus2 voltage changes from 1 $p.u$ to

1.11 $p.u$ at $\tau = 1$ s, suddenly. In order to recover Bus2 voltage close to the rated voltage, the

current tap position needs to shift to a lower one. Bus2 voltage error is 0.11 $p.u$, which is

twice higher than 0.05 $p.u$, thereby requiring the tap to change twice as the voltage

decreases from 1.11 $p.u$ to 1.01 $p.u$. Finally, Bus2 voltage decreases to 1.01 $p.u$.

5.2 Modeling of OLTC Systems via Traditional Method

5.2.1 Traditional Method

According to [Zhao, 2006] and [Hiskens, 2000], a hybrid system can be described as

continuous and discrete-event system based on an algebraic method. The model of the

continuous system can be described as follows:

$$\dot{x} = f(x, y, z) \tag{5.2}$$

$$g(x, y, z) = 0 \tag{5.3}$$

where x presents a continuous dynamic state variable; y is an algebraic state variable; and z

is a discrete state variable. Equation (5.2) is a power system's differential algebraic

equation. Equation (5.3) is guard conditions representing the protection relay operating

conditions, on-load transformer tap adjusting conditions, etc.

The discrete event system is represented by a four tuples,

$$G = (Q, \Sigma, \delta, q_0) \tag{5.4}$$

where Q is the set of states in G, $q = (q_1, \ldots, q_N)^T \in Q$ is a state vector, $q_0 \in Q$ is the initial state of G, and q_i denotes the i-th state of the discrete event system.

Σ is the set of events in G, and $e \in \Sigma$ denotes an event.

$\delta: Q \times \Sigma \rightarrow Q$ is a state transition function of G.

On the basis of an algebraic method, the system is described as two parts, continuous and discrete ones. A triggered event can impact the system and change its dynamic parameters. It can be shown as a piecewise function. In order to describe this complex system, the functions of pre-event and post-event are needed. Since it is hard to describe both discrete event and continuous behavior in a single equation, their descriptions are separated.

5.2.2 OLTC System Modeling

The descriptions of discrete event and continuous behavior are described as follows. We use the OLTC system in Figure 5.1 as an example to illustrate the algebraic method. Discrete events can be described as:

$$\Sigma = (e_1, e_2, e_3) \qquad (5.5)$$

where e_1 represents that Bus2 voltage increases to 1.11 $p.u$ at $\tau = 1$ s; e_2 represents the first

tap change at $\tau = 1$ s; and e_3 represents the second tap change at $\tau = 1.1$ s.

$$Q = (n) \qquad (5.6)$$

where n represents the current tap position; and n^+ denotes the tap position after an event

occurs.

The continuous behaviors are derived as follows:

$$\Delta V = V_2(\tau) - V_{rate} \qquad (5.7)$$

$$V_2(\tau + \Delta\tau) = V_2(\tau) + \Delta k \cdot f(\Delta V) \cdot V_1 \qquad (5.8)$$

$$n^+ = n + n_{step} \cdot f(\Delta V) \qquad (5.9)$$

$$f(\Delta V) = \begin{cases} -1, & \Delta V \geq 0.05 \ p.u \\ 0, & -0.05 \ p.u < \Delta V < 0.05 \ p.u \\ 1, & \Delta V \leq -0.05 \ p.u \end{cases} \qquad (5.10)$$

where $\Delta\tau$ represents a very small time interval; n_{step} represents that n_{step} tap positions are

changed after one tap change. In this example, n_{step} is assumed to be 1. Because Bus1

voltage equals the terminal voltage of the generator, V_1 is assumed to be 1 $p.u$ as well. After

analyzing the process of the tap change, a piecewise function is obtained as follows:

$$V_2(\tau) = \begin{cases} 1 \ p.u, & 0 \ s \le \tau < 1 \ s \\ 1.11 \ p.u, & \tau = 1 \ s \\ 1.06 \ p.u, & 1 \ s < \tau \le 1.1 \ s \\ 1.01 \ p.u, & 1.1 \ s < \tau \le 25 \ s \end{cases} \qquad (5.11)$$

Figure 5.2 shows a logic framework for tap changing. Figure 5.3 shows the result of the traditional method.
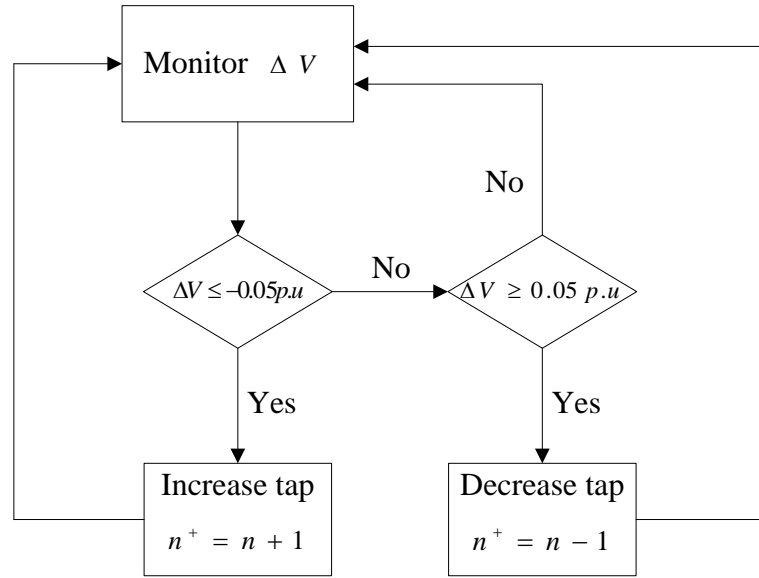
Figure 5.2 A logic framework for tap changing.
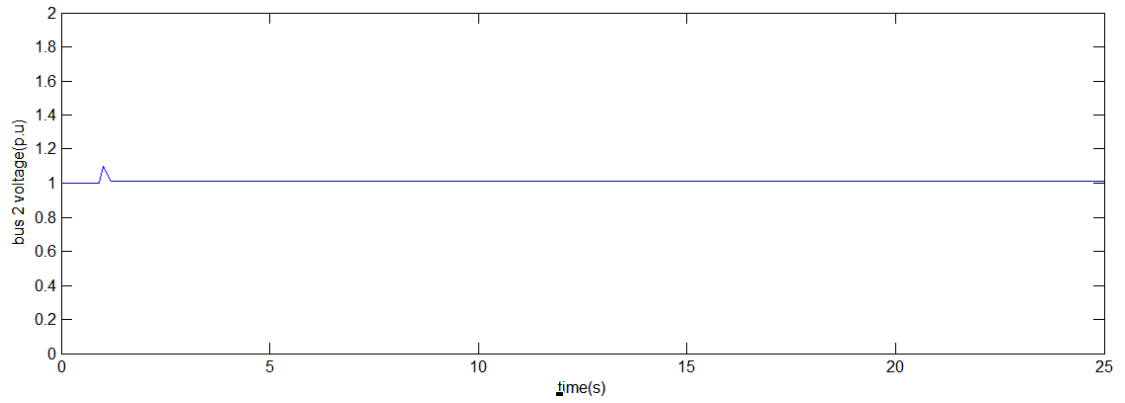
Figure 5.3 The simulation result of Bus2 voltage based on the traditional method.

According to the result, Bus2 voltage reaches 1.1 *p.u.* at time $\tau = 1s$. After two tap changes,

Bus2 voltage becomes 1.01 *p.u.*

5.3 Modeling of OLTC with Hybrid Petri Nets

5.3.1 Modeling of OLTC Based on HPN

OLTC is a hybrid system. It represents a continuous behavior for the voltage change.

However, the tap change from one tap position to another is a discrete event. A proposed

HPN model is shown in Figure 5.4. The meanings of places and transitions are given in

Table 5.1.
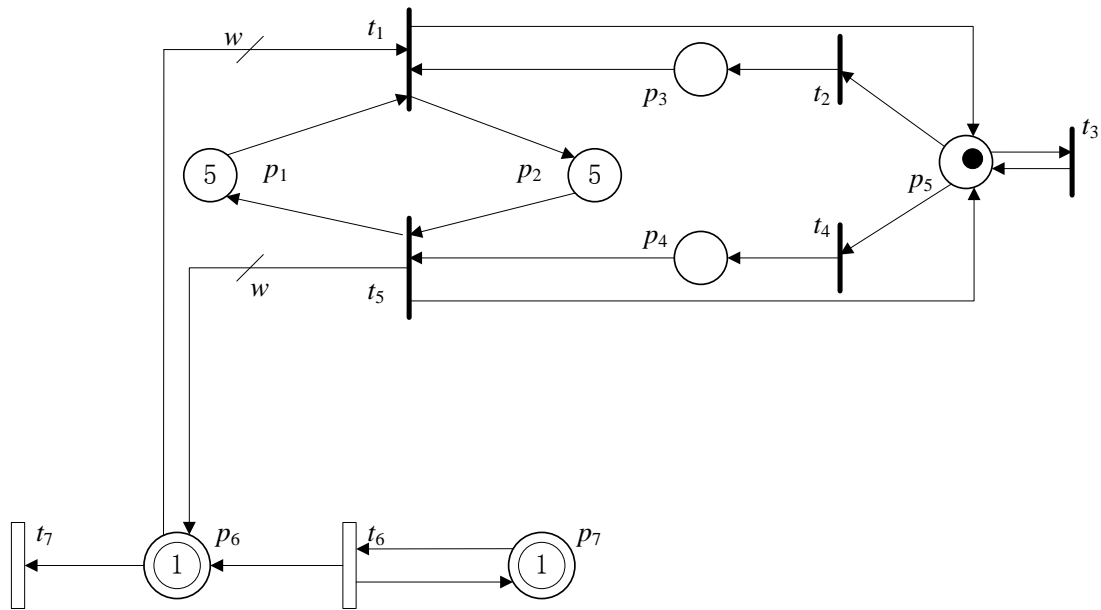
Figure 5.4 An HPN model of OLTC.

In this HPN, p_1 and p_2 are two discrete places with their capacities as 10. If they reach their maximum capacities, the input transitions become disabled and thus cannot fire. Meanwhile, the token count of p_1 represents the tap position. Similarly, the token count of p_2 represents the available tap position. A weight w is marked to the arc that connects a discrete place to a continuous one. In a traditional PN, w is a natural number. In order to adapt to a real power system, w is assumed to be a positive real number. The process of tap position changing can be described as follows:

The initial marking is set as [5 5 0 0 1 1 1]. It represents that the current tap position is 5, and the transformer has 5 more positions available. Meanwhile, $V_1=V_2=1$ p.u, initially.

Table 5.1 Meanings of Places and Transitions of the HPN Model of an OLTC System

p_d	p_1	Tap position
	p_2	Available tap position
	p_3	$\Delta V \geq 0.05$ p.u
	p_4	$\Delta V \leq$ -0.05 p.u
	p_5	Voltage detector (monitor the system voltage)
p_c	p_6	Bus1 voltage
	p_7	Bus2 voltage
t_d	t_1	Tap position shift to a lower position
	t_2	$\Delta V \geq 0.05$ p.u
	t_3	-0.05 p.u$<\Delta V < 0.05$ p.u
	t_4	$\Delta V \leq$ -0.05 p.u
	t_5	Tap position shift to a higher position
t_c	t_6	Power flows from Bus1 to Bus2
	t_7	Power flows from Bus2 to the load

When $\Delta V \leq$ -0.05 $p.u$, t_4 is enabled. A token goes to p_4 from p_5. Then t_5 is enabled to

shift the tap to a higher tap position. When t_5 fires, quantity w is added into continuous

place p_6. On the contrary, when $\Delta V \geq$ 0.05 $p.u$, t_2 is enabled. A token goes to p_3 from p_5,

then t_1 is enabled. Its firing moves one token from p_1 to p_2, which means that the tap

position is shifted down and the available tap position increases by one. Meanwhile, the

token in p_3 goes to p_5. At the same time, quantity w is eliminated from continuous place p_6.

In this model, w is assumed to be $|\Delta k|$ (Δk=0.05).

For continuous transition t_6, because the terminal voltage of the generator is a

constant value, the firing speed is set as constant: $v_1(\tau)$=0.2 $p.u/s$;

For continuous transition t_7, because load decreases at time $\tau = 1$ s, bus2 voltage is

increased to 1.11 $p.u$. Then firing speed of t_7 is set as:

$$v_2(\tau) = \begin{cases} 0.2 \ p.u/s, & 0 \ s \leq \tau < 1 \ s \\ 0.09 \ p.u/s, & \tau = 1s \\ 0.2 \ p.u/s, & \tau > 1s \end{cases} \tag{5.12}$$

In addition, when the proposed HPN model is compared with the PN model

mentioned in [Paruchuri, 2005], it is simplified by using finite capacity places to replace

the infinite capacity places. In the PN model, it just models the behaviors of tap change.

However, besides the modeling of the behaviors of tap change, the proposed HPN model

also simulates the behaviors of the voltage detector and the voltage variation of a microgrid.

5.3.2 Simulation Result

Figure 5.5 shows the simulation result based on the proposed HPN. It describes the voltage variation, tap position and available tap position. In this example, Bus2 voltage is set as 1.11 *p.u* and voltage variation of each level is 0.05 *p.u*. Thus, tap position needs to be changed twice, and finally the system voltage is 1.01 *p.u*. Initially, the tap position is 5 by holding 5 tokens in p_1, and then the tap position is shifted to a lower position. After two tap changes, the tap position is 3 by holding 3 tokens in p_1. Meanwhile, there are 7 tokens in p_2, which means that the transformer has 7 available tap positions. The upper plot of Figure 5.5, which is based on the proposed HPN, is the same as Figure 5.3 which is based on the algebraic method.
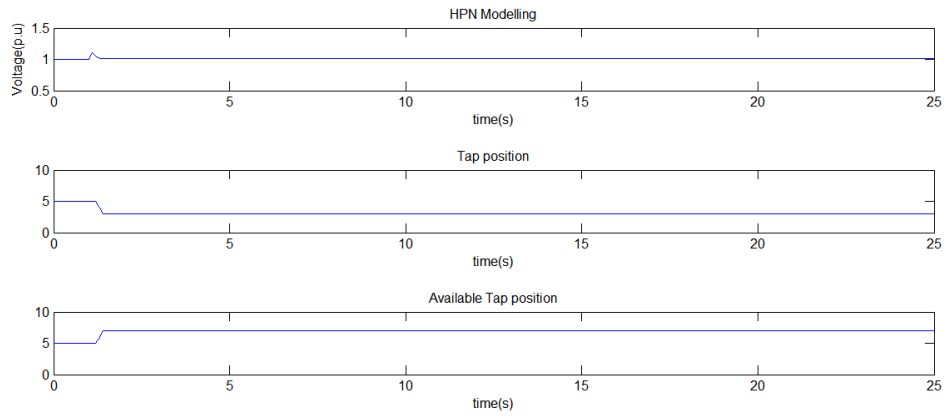
Figure 5.5 Simulation results of the HPN model.

In Figure 5.5, we assume that the tap change is an ideal process that experiences no time delay. But in a real power system, during the interval process of tap change, the transformer needs a motor to change the tap position, which requires to consume time. In this proposed HPN model, we just need to associate a time delay with t_1 or t_5 to mimic a delayed process of tap changing.
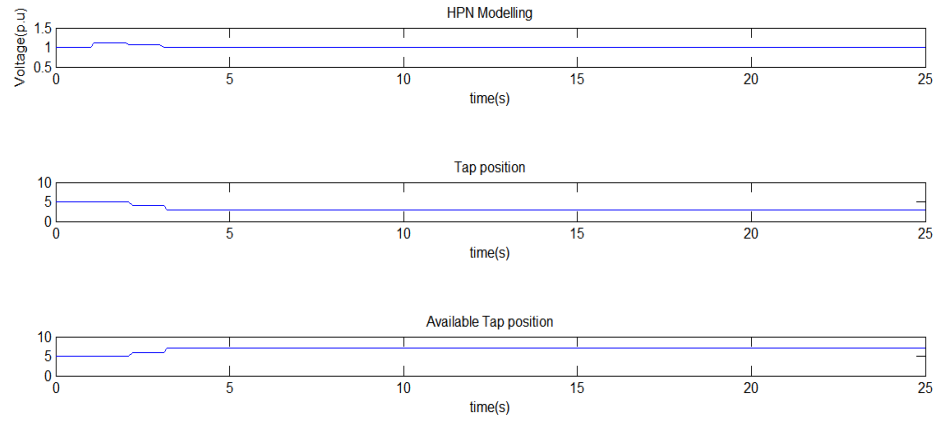
Figure 5.6 Simulation results of the HPN model with time delay.

Figure 5.6 shows the system behavior with 1 second delay before the system changes the voltage. The tap position and available tap position are shown in the middle and lower plots of Figure 5.6. The comparison results between the existing algebraic and HPN methods is shown in Table 5.2. The HPN has a clear advantage in clearly describing a hybrid system than the algebraic method. It is an integrated model exhibiting both discrete event and continuous behavior of a power system.

Table 5.2 Comparison Method

	Algebraic Method	HPN
Description of Continuous behavior and Discrete event	Separated	Combined
Dynamic function	Pre-event function, Post-event function	Firing speed function
Visualization	No	Yes

CHAPTER 6

CONCLUSION

Controlling multiple distributed generators (DGs) and modeling both discrete event and continuous behavior of a microgrid are two important research issues that are widely discussed. This thesis proposes a Petri net method to address these two issues. As the important extensions of ordinary Petri nets (PN), finite capacity Petri nets and hybrid Petri nets are adopted to build up concise mathematical models for microgrids. The concepts of Petri nets and extended Petri nets are given in Chapter 3 with some examples of PN models. In addition, an HPN model of a 4-DG microgrid as an example is proposed to simulate a microgrid. Some piecewise constant curves of daily load demand, energy produced by wind turbine and photovoltaic cell as examples are used to draw its reachability graph.

Multi-V/f control is a traditional control method to address the first issue, which depends on the system frequency variant. Chapter 4 proposes a PN model to control a 3-DG system. When it is compared with the traditional multi-V/f control, the model depends on not only the system frequency but also the states of DGs, enabling the system to possess a long stable time interval. However, there are still some limitations. Firstly, the proposed PN model is based on an ideal system. Thus, this model needs to be tested and realized to adapt to a real system. Secondly, since DGs are different, such as photovoltaic cells and diesel generators, new requirements have to be considered. The proposed model is for a 3-DG system. If a system has more than three DGs, the model does not work but has to be extended.

An HPN model is proposed to model an On-Load Tap Changing (OLTC) transformer system in Chapter 5. Then, it is compared with a traditional method based on the algebraic method. The advantages of the proposed HPN model are as follows: 1) this model can describe both discrete event and continuous behavior in an integrated manner; 2) only firing speed function is needed to model a hybrid system; 3) to compare with the algebraic method, this model has an advantage in easy visualization. Meanwhile, the HPN model of an OLTC system is compared with the PN model of the same system. The former one can describe more behaviors of an on-load tap changing system than the latter one. However, in this thesis, the limitation is that only the OLTC system is modeled. Since a microgrid is such a complex system, more complex behaviors need to be modeled by HPN.

In the future work, the PN method is required to model complex behaviors of a microgrid. First, comparing with the piecewise constant curve, more complex curves, such as a stochastically changing curve, are needed to model a complex microgrid. Second, a general PN model is required to model the control of an n-DG system. Moreover, some other hybrid systems, such as fault diagnosis, are required to be modeled.

REFERENCES

Aydin, B. (2014). SWOT analysis of renewable energy. In *Proc of 2014 IEEE International Conference and Utility Exhibition on Green Energy for Sustainable Development (ICUE)* (pp. 1-7).

Banerji, A., Sen, D., Bera, A. K., Ray, D., Paul, D., Bhakat, A., & Biswas, S. K. (2013). Microgrid: A review. In *Proc. of 2013 IEEE Global Humanitarian Technology Conference: South Asia Satellite (GHTC-SAS)* (pp. 27-35).

Barsali, S., Ceraolo, M., Pelacchi, P., & Poli, D. (2002). Control techniques of dispersed generators to improve the continuity of electricity supply. In *Proc. of 2002 IEEE Power Engineering Society Winter Meeting* (Vol. 2, pp. 789-794).

Chamorro, H. R., & Jimenez, J. F. (2012). Use of Petri nets for load sharing control in distributed generation applications. In *Proc. of 2012 IEEE 3rd International Symposium on Power Electronics for Distributed Generation Systems (PEDG)* (pp. 731-736).

Chamorro, H. R., Ordonez, C. A., & Jimenez, J. F. (2012). Coordinated control based Petri nets for microgrids including wind farms. In *Proc. of 2012 IEEE Conference on Power Electronics and Machines in Wind Applications (PEMWA)* (pp. 1-6).

Chan, Y. K., & Gu, J. C. (2011). Modeling and simulation of microturbine and renewable energy resources for distributed generation system. In *Proc. of 2011 IEEE 8th Asian Control Conference (ASCC)* (pp. 590-595).

David, R. (1997). Modeling of hybrid systems using continuous and hybrid Petri nets. In *Proc. of 1997 IEEE conference on Petri Nets and Performance Evaluation* (pp. 47-58).

Dimeas, A. L., & Hatziargyriou, N. D. (2005). A MAS architecture for microgrids control. In *Proc. of 2005 IEEE 13th International Conference on Intelligent Systems Application to Power Systems* (pp. 1-5).

Gao, C., He, X., Wang, H., & Li, P. (1999). Modeling, safety verification and optimization of operating procedures in process systems using hybrid Petri nets. In *Proc. of 1999 IEEE International Conference on Systems, Man and Cybernetics* (Vol. 1, pp. 854-859).

Hartono, B. S., & Setiabudy, R. (2013). Review of microgrid technology. In *Proc. of 2013 IEEE International Conference on Quality in Research* (*QiR*) (pp. 127-132).

Hiskens, I. A., & Pai, M. A. (2000). Hybrid systems view of power system modelling. In *Proc. of 2000 IEEE International Symposium on Circuits and Systems* (Vol. 2, pp. 228-231).

Hruz, B., & Zhou, M. C. (2007). Modeling and Control of Discrete Event Dynamic Systems, Springer: London, UK.

Kamel, R. M., Chaouachi, A., & Nagasaka, K. (2013). Three control strategies to improve the microgrid transient dynamic response during isolated mode: A comparative study. *IEEE Transactions on Industrial Electronics 60*(4), 1314-1322.

Li, Z. W., & Zhou, M. C. (2009) Deadlock Resolution in Automated Manufacturing Systems: A Novel Petri Net Approach, Springer: New York, NY.

Lin, Z., Wen, F., Chung, C. Y., & Wong, K. P. (2006). A survey on the applications of Petri net theory in power systems. In *Proc. of 2006 IEEE Power Engineering Society General Meeting* (pp. 1-7).

Molina, M. G., & Mercado, P. E. (2008). Modeling and control of grid-connected photovoltaic energy conversion system used as a dispersed generator. In *Proc. of 2008 IEEE/PES Transmission and Distribution Conference and Exposition: Latin America* (pp. 1-8).

Paruchuri, V. K., Davari, A., & Feliachi, A. (2005). Hybrid modeling of power system using hybrid Petri nets. In *Proc. of 2005 IEEE Thirty-Seventh Southeastern Symposium on System Theory* (pp. 221-224).

Peas Lopes, J. A., Moreira, C. L., & Madureira, A. G. (2005). Defining control strategies for analysing microgrids islanded operation. In *Proc. of 2005 IEEE Russia Power Tech* (pp. 1-7).

Peas Lopes, J. A., Moreira, C. L., & Madureira, A. G. (2006). Defining control strategies for microgrids islanded operation. *IEEE Transactions on Power Systems 21*(2), 916-924.

Piagi, P., & Lasseter, R. H. (2006). Autonomous control of microgrids. In *Proc. of 2006 IEEE Power Engineering Society General Meeting* (pp. 8-15).

Qiao, Y., Wu, N. Q, & Zhou, M. C. (2013). A Petri net-based novel scheduling approach and its cycle time analysis for dual-arm cluster tools with wafer revisiting. *IEEE Transactions on Semiconductor Manufacturing 26*(1), 100-110.

Sava, A., Adjallah, K. H., & Lagaza, H. (2014). Hybrid Petri nets for modeling and control of mulit-source energy conversion systems. In *Proc. of 2014 IEEE 2nd International Conference on Control, Decision and Information Technology (CoDIT)* (paper #182, pp. 1-6) Metz, France.

Tian, S., Tong, X.Q., & Ren, B.Y. (2010). The Control Strategy Based on Improved Droop Method of Microgrid-Connected Inverters. In *Proc. of 2010 IEEE International Conference on Electrical and Control Engineering (ICECE)* (pp. 5700-5703).

Wang, Y., Tan, K. T., & So, P. L. (2013). Coordinated control of battery energy storage system in a microgrid. In *Proc. of 2013 IEEE Asia-Pacific Power and Energy Engineering Conference (APPEEC)* (pp. 1-6).

Xu, C. Q., Li, T. M., Dong, R. N., & Jia, G. Z. (2013). Research on energy-hub control method of micro-grid based on multi-agent & Petri nets. In *Proc. of 2013 IEEE Fourth International Conference on Intelligent Systems Design and Engineering Applications* (pp. 468-471).

Xu, W. H., Liao, Z. W., Huang, S. X., & Wang, G. (2005). A model of HVDC control system based on hybrid Petri net. In *Proc. of 2005 IEEE/PES Transmission and Distribution Conference and Exhibition: Asia and Pacific* (pp. 1-6).

Zhang, X. A., Zhang, X. C., Tang, Y. L, Kong, B. L., & Cui, L. Y. (2014). Research on adaptive master-slave control of islanded microgrid. *Power System Protection and Control* (Vol. 42, No 2, pp. 81-86).

Zhao, H. S., Mi, Z. Q., & Ren, H. (2006). Modeling and analysis of power system events. In *Proc. of 2006 IEEE Power Engineering Society General Meeting* (Vol. 26, No. 22, pp. 11-16).

Zhou, M. C. (Ed.), (1995). Petri Nets in Flexible and Agile Automation. Kluwer Academic Publishers: London, UK.

Zhou, M. C., & DiCesare, F. (1993). Petri Net Synthesis for Discrete Event Control of Manufacturing Systems. Kluwer Academic Publishers: London, UK.

Zhou, M. C., & Fanti, M. P. (Ed.), (2005). Deadlock Resolution in Computer-Integrated Systems, Marcel Dekker: New York, NY.

Zhou, M. C., & Venkatesh, K. (1998). Modeling, Simulation and Control of Flexible Manufacturing Systems: A Petri Net Approach. World Scientific: Singapore.